CHIMERE-2017 : from urban to hemispheric chemistry-transport modeling
by S. Mailler et al.

Answer to Anonymous Reviewer 1

This manuscript details the recent updates made to the CHIMERE chemical transport model to extend its capability to include urban and hemispheric modeling. As pollution concentrations have fallen in many areas in the past couple decades, the problem of air pollution has expanded from being primarily a local/regional issue to a more hemispheric/global issue. Therefore, having air quality models capable of simulating the hemispheric to local scale are becoming more important. This work attempts to detail the vast number of updates made to the CHIMERE modeling system in order create a more versatile modeling system. The authors and developers of the model should be commended on what was surely a very large undertaking to update almost every aspect of the modeling system. The manuscript also includes a section that attempts to evaluate the performance of the new modeling system, which in my opinion is the weakest section of the manuscript.

First of all, we would like to thank Reviewer 1 for his/her careful reading of our paper and many useful comments, and evaluating in a careful and fair way the strengths of the manuscript and its limitations.

Please note that the title of the paper has been updated to CHIMERE-2017 instead of CHIMERE-2016 since a new model version has been issued, with only bugfixes from the 2016 version. All the simulations have been redone with this corrected version, which does not bring any change in the discussion since the changes are only small bugfixes.

Below are, in blue, the comments and requests by Reviewer 1, in black our answers, and in green the description of the corresponding changes that have been brought to the Manuscript, when relevant.

My general comment on the evaluation of the CHIMERE-2016 modeling system is that it really only provides model performance metrics for a very coarse modeling domain (0.5 X 0.5 degree).

Yes, this is true. However, we refer more explicitly in the last version of the paper to recent studies (e.g. Markakis et al., 2015, Terrenoire et al. 2015) giving thorough validations of the model for regional/urban scale, including an article by Bessagnet (2016) describing results from the multimodel comparison EURODELTA III project, which gives detailed information about model performance and comparison to other CTMs.

This is done in the introduction, p. 2, l. 25-49

In addition, wherever the model performance is poor, the authors simply seem to blame the emissions for the poor performance.

This maybe seems like that but, for example regarding SO2, what we actually blame for poor performance is not the emission inventory itself, but rather the vertical disaggregation profiles, which are model developers' choice (our choice) but are highly uncertain, and assume that vertical emission

profiles are uniform in time independantly of meteorology etc. Which is of course questionable. This is now mentioned explicitly as a model limitation (p. 18, l. 22-34)

For NOx emission, we now refer more precisely to Terrenoire (2015) (p. 18, l. 13-21) who makes a more precise statement about possible missing emissions, but of course we are aware that emissions are far from being the only source of error in simulated concentrations, and we hope that this appears in the manuscript.

In my opinion, the evaluation provided does little to provide real faith that the new modeling system can accurately simulate air pollution across a multitude of scales. Also, the volcanic ash case study simulation provided seems only to establish that the model physics does not fail while traversing the southern hemisphere. No evaluation of the actually particle concentrations for the case study is really provided, so it's not clear whether the model can actually simulate the fate of the emitted ash particles (e.g. effects of particle transformation and deposition) with any real accuracy.

This is correct, but actually, when changing the model structure from lat-lon to other coordinate system allowing modelling of circumpolar transport, the most challenging part was to actually obtain a model that was able to perform the transport without errors, because the rewriting of the transport schemes was using a very different discretization principle than in previous model version, so this simulation is aimed at showing that the model is able to have the volcanic plume arrive at the right time at given places where it has been actually observed. This is what we intend to show by comparing our results to published reports about the chronology of the Puyehue ash plume in a variety of locations.

Simulating the right concentrations for ash and the right AOD is more dependant on the model forcing by emitted volumes of ash and their size distribution, which are so uncertain that modellers can just adjust them by trial and error to obtain the desired concentrations and AODs (for example, the m_{63} parameter that permits to evaluate the fraction fo fine ash / total ash can vary from about 0.01 to about 0.6 from one eruption to another and it is very difficult to have reliable measurements of this parameter). For these reasons, we chose to just have a first estimate of the emissions according to published data/methods, and focus on the chronology, because the part of the model that was modified most deeply in updating for regional to hemispheric version is the transport, so this is what actually needed to be checked, and is in our opinion verified since the modelled plume is back to the Chilean coast and at the correct location on June 13/14 as observed.

However, we hope to obtain better estimates of ash and SO2 emissions by working with specialists of volcanic emissions and perform a comparison of AOD and SO2 columns in a further study.

It would very useful to have a much more detailed evaluation of the modeling system, including simulations at various horizontal grid resolutions and domain sizes (e.g. urban at fine grid resolution, regional at moderate grid resolution, and hemispheric at coarse model resolution). This may be too much to add to this manuscript, so perhaps it would be better if the authors tackled this as a Part I/Part II series, with Part I describing the updates to the modeling system (as has been done), and Part II providing a detailed model evaluation of the system. I think this would end up being a much more useful set of papers to potential CHIMERE users in my opinion. As it stands, I don't feel like the evaluation in the manuscript provides enough support for the amount of work that was done in updating the model.

In our view, this manuscript is a model description manuscript more than model evaluation, since a

number of studies already use the CHIMERE model and compare it to observations and to other comparable models, giving to the interested users a detailes view of the performance of the model depending on the species, the resolution, etc. We added some information in this sense in the revised version, including more references to detailed evaluation papers such as Terrenoire (2015) or Bessagnet (2016) . Even though these papers use earlier versions of the model, the model performance in its "classical" regional configuration only evolves smoothly with time even when lots of new developments are included, this is also the case between the described version and earlier versions that have been thoroughly evaluated. Therefore, the focus in this paper is not put on evaluating a strong increase in model performance, which is not the case (the evolution of modelling scores from one version to the next is slow and smooth), but a change in the scope of the model, including more processes, and extending the capabilities in terms of domain size to the hemispheric scale. This precision of the scope of the manuscript can be found in the introduction of the revised paper, p. 2, l. 29-46.

I've provided a number of specific comments in the PDF provided with this review.

Thank you very much, these specific comments have been adressed directly when it was typos or propositions for rephrasing (thank you very much for signaling them), for more substantial comments you will find the answers below.

p. 2, l. 14 : Missing reference for MELCHIOR chemical scheme

The original reference in to the PhD thesis of Mireille Lattuati :
Lattuati, M.: Contribution à l'étude du bilan de l'ozone troposphérique à l'interface de l'Europe et de l'Atlantique Nord: modélisation lagrangienne et mesures en altitude, Phd thesis, Université Pierre et Marie Curie, Paris, France, 1997

However, the model is extensively described with lists of species and reactions in a more recent paper by Menut et al. (2013), which is now cited, easier to find and in English (cited for that purpose on p. 2, l. 70).

p. 3, l. 13-15 : Important to note here that in the current offline configuration no radiative feedback effects to the meteorology are available, which can be important when simulating aerosol effects, particularly on the global scale.

The following sentence has been added : "Another important point is that even though the processing of meteorological input has been changed as described here, the present version offers does not take into account any radiative or microphysical feedback of atmospheric chemistry on meteorology." (p. 2, l. 76-79)

p. 3, l. 26 : It would be useful to clarify exactly what is meant by "workers". In this case, the processors doing the grid computations.

This has been done :by replacing "workers" by "the various slave processes that performed the actual gridded calculations" (replacing "workers" by "slaves" is a requirement of Reviewer 2)

p. 4, l. 3-6 : This would seem an appropriate place to discuss the runtimes for some different model configurations (e.g. regional vs. global with varying horizontal and vertical grid spacings). I don't recall

the model runtime being discussed in detail anywhere else in the manuscript.

While we agree that it would be interesting to provide such a discussion, we did not perform the necessary simulations and computational tests to do it, which would involved a controlled computational environment – particularly regarding i/o processes that may be competing with the test simulations, tests with different resolutions, different numbers of cores, etc.

p. 8, l. 14-15 : This is very low model top for a model simulation, particularly at the continental/hemispheric scale. There needs to be some discussion of how the boundary at the top of the model is handled, and that in the case of such a low model top, the model providing the boundary conditions extremely important to accurately simulating on such a large scale.

The statement in l. 14-15 is as follows : "The pressure of the top of the model, p_{top}, typically from 500 hPa for studies at urban/regional scales to 200 hPa for continental/hemispheric scale studies."

While these pressure levels of model top would be very low for a meteorological simulation, making the choice of the boundary conditions critical, we have the feeling that for chemistry-transport simulations this is not so because most trace gases have either very small or slowly variable concentrations at this altitude, with the notable exception of ozone. Therefore, the boundary conditions at the model top and boundaries are taken from climatologies, typically from LMDZ-INCA simulations for all species except for mineral dust for which climatological concentrations are taken from GOCART.
Note that the model top is an adjustable parameter and has only the meteorological driver as constrainst.
In our case and in this revised version, the hemispheric simulation was actually performed with a model top of 100hPa. The sentence with 'typically' was changed and is now: "The pressure of the top of the model, p_{top}, can be freely set by the user with typical values from 500 hPa for studies at urban/regional scales to 100 hPa for continental/hemispheric scale studies." (p. 6, l. 49-52)

p. 10, l. 12-17 : So the user is able to define their own splits for these species if they wish?

These speciation tables are described in the model documentation, and the users may modify them to take into account their own splits if they wish top use other splits than described here.

p. 10, l. 20-22 : Is there a lower limit to a user specified layer one model height? What if a user specifies a very low layer one height?

Actually the statement was erroneous : Residential emissions are affected not to the first model layer but to a layer between 0 and 20m height, which might overlap on the second model layer if the first model layer is very thin. In the revised version, we provide a reference to Terrenoire et al. (2015) where the detailed profiles that are used for vertical disaggregation are presented. (p. 7, l. 53-57)

Regarding the precise question the Reviewer is asking, there is no lower limit to the user-specified thickness of the first layer model. As specified p. 6, l. 42-46, this parameter is freely set by the user. It is the user responsability to choose values such that the model configuration is reasonable.

p. 10, l. 23 : How exactly is the layer in which these emissions are emitted determined? Is any plume-rise calculation still being performed? It's not clear from the text exactly what method is being used to determine the layer the emissions are emitted.

No plume-rise is applied, fixed emission profiles are used for each SNAP sector, as described in Terrenoire (2015). The following sentence has been added :
The vertical distribution profiles that are used for each SNAP (``Selected Nomenclature for Air Pollutants") sector are constant profiles depending only on the SNAP sector, and are presented in Terrenoire (2015) (p. 7, l. 53-57).
The absence of a plume-rise representation is now explicitly mentioned p. 18, l. 30-34 as a possible reason for the lack for too weak SO2 concentrations.

p. 15, l. 11 : Why is that? Does resuspension not also occur over non-urbanized surface? Please explain the rational for only applying the resuspension over urbanized surfaces.

The resuspension process differs from the emissions. In the model, we consider only the traffic-related resuspension from the traffic-related emissions. This is why this source is taken into account only in the PPM species (anthropogenic) and in urbanized areas. But we agree with the Reviewer than resuspension process may occur in other environment. This is just not taken into account for the moment in this model version. The title of this paragraph has been changed to “traffic-related resuspension”, making it clear that not all resuspension processes are taken into account.

p. 17, l. 9 : What specifically are "various environments"? Please give at least several examples here.

The following sentence has been added (p. 12, l. 21-25):

If the role of halogen chemistry was traditionally considered limited to the marine boundary layer, recent observations have shown significant $ClNO_2$ concentrations from few ppt in Mid-Continental Urban Environment (Mielke, 2011) to 2000 ppt in the Coastal Marine Boundary Layer (Riedel, 2012).

p. 18, l. 10-11 : How reasonable is this assumption? Is there a reference available? Or is it stated in Nenes et al.?

Yes, ISORROPIA is a model for inorganic aerosols only, and its original version described in Nenes et al. (1998) makes the hypothesis that mineral dust and organic aerosols are not hygroscopic. Even though ISORROPIA II (Nenes et al. 2007) takes into account the solubility of some components of mineral dust, this is not taken into account into CHIMERE, partly because CHIMERE so far does not include information on the composition of mineral dust.

p. 19, l. 10 : Already referenced and explained in the previous section.

This has been corrected, thanks.

p. 21, l. 5 : Please elaborate on what condensed phases of water (e.g. ice particles, snowflakes, graupel, etc.) are used in the calculation of extinction from cloud water and ice. How are the optical properties determined from cloud water and ice?

Following the recommandations of the Fast-JX developers, the effective size of ice particles is estimated following Heymsfield (2003), J. Applied. Meteorol. :

```
REFFI = 164. * (IWC**0.23)
```

Where Reff,i is the effective radius of ice particles, and IWC is the ice content of the atmospheric particles (g/m3).

Regarding water droplets, their radius is estimated also following the recommandations of fast-JX developers, as 9.60 µm for clouds at low altitudes (below 810 hPa), 12.68µm for high clouds (above 610 hPa), and linearly interpolated between these two values for intermediate altitudes. We are not aware where these recommendations come from, however, they are consistent with the typical radius of cloud water droplets.

This is now mentioned in detail in the article (. 14, l. 36-44).

p. 21, l. 11-12 : Does light extinction from clouds include cloud overlap or overlay? If so, how?

No. Light extinction for clouds unfortunately does not take into account the possibility of fractional cloud covers and the possible overlaps between successive cloud layers. The cloud fraction is not read from the meteorological model, and the cloud layers are assumed to be horizontally uniform in each grid cell. However, the succession of various cloud layers over the vertical dimension is taken into account in a complete way by the Fast-J radiative module, including the reflexion and diffusion of upward and downward fluxes by each cloud layer.

p. 23, l. 3 : Clarify what mixing model is used to calculate the optical properties of the aerosol size bins and why. The paper may give conflicting information. Section 5.3.3 states that an external mixing model is used but section 5.2.2 states that an internal mixing model is used for the wet aerosol diameter and density. If internal model determines the optical properties, give more details about the type of internal model such as volume weight average, core-shell, etc.

For optical properties, external mixing is assumed, while for other processes (thermodynamics etc.), the model assumes internal mixing. It is true that this choice can be surprising. It is well-known that the assumptions on the mixing state of aerosols can have an impact of their radiative properties, but in the CHIMERE model, so far external mixing is assumed, and each species interacts with solar radiation according to its own refractive index, and the corresponding terms of the Legendre expansion for its phase function.

p. 23, l. 10 : Please provide a reference for the ADIENT project.

The following sentence has been added :
The refractive indices reproduced in Table 5 are the ones provided along with the model, essentially based on the values compiled in the framework of the ADIENT project (http://www.reading.ac.uk/adient/refractiveindices.html, visited Jan. 17, 2017, as described by the corresponding technical report by E. J. Highwood (www.reading.ac.uk/adient/REFINDS/Techreportjul09.doc}, visited Jan. 17, 2017) – p. 15, l. 34-38

Table 4 : Please state why Table 4 assigns OCAR refractive indicies associated with Brown Carbon. What type of organic material does OCAR represent?

As for other species, we relied on the data provided by the ADIENT project and the corresponding technical report which gives the following explanations about Organic carbon :

“This discussion applies to the component of organic aerosol that is not black carbon and generally derives from fossil fuel burning. Since

the composition of this aerosol depends on combustion type and material it is problematic to prescribe parameters suitable for all occasions. Atmospheric organic crabon is often described as HULIS – Humic-Like Substances. HULIS samples have been recorded with refractive indices of 1.595-0.049i (Pollution, Dinar et al, 2007), 1.622-0.048i (wood burning smoke, Dinar et al 2007), 1.56-0.003i (rural continental, Dinar et al, 2007), 1.65-0.0019i (biomass burning, Hoffer et al, 2006), 1.45-0.001i (Kreckov et al, 1993 – used in ADRIEX), 1.53-0.0055, (Koepke et al, 1997, used for POM in ECHAM). Measurements of the absorption properties of atmospheric HULIS use a variety of techniques to extract the HULIS from the aerosol. Some of these techniques can enhance the hydrophilic compounds for pollution and smoke samples. Perhaps for this reason, Swannee River Fulvic Acid (SRFA) has been used as proxy for atmospheric HULIS in numerous studies (e.g. Dinar et al, 2007) as it is available for laboratory measurements although some caution must be attached. Laboratory SRFA has a density of 1.47 g cm-3 and a refractive index of 1.634-0.021i at 532nm. Other groups use information from observations of biomass or fossil fuel burning to constrain their optical properties. For example, HADGEM2, the Met Office climate model, has separate optical properties for FFOC (fossil fuel organic carbon), SOA (secondary organic aerosol), and fresh and aged biomass aerosol. The real part of the refractive index for aged OC in HadGEM2 is taken to be the same as that for Biomass Burning (which is constrained by measurements at some wavelengths – 1.54 at 550nm) and the imaginary part of the refractive index is assumed to be wavelength independent at -0.006 (compared to that for aged biomass burning of 0.02 at 550nm). This value for OC is at the low end of the estimates for absorption from HULIS measured in the atmosphere and also lower than the absorption from SRFA.
It is clear that there is a range of uncertainty in the imaginary part of the refractive index that is appropriate for organic carbon. Even if one accepts that HULIS is appropriate, then this varies according to source and location. The aging process is also a complicating factor. The situation becomes more difficult if values at wavelengths other than 550nm are required. Kirchstetter et al (2004) report that the spectral dependence of light absorbing aerosols is dependent on the temperature and completeness of combustion – with high temperature combustion processes (such as diesel burning) exhibiting much less spectral dependence of absorption. They suggest a wavelength dependence of the mass absorption efficiency according to $\sigma = K\lambda^{-\alpha}$ where α is the absorption angstrom exponent and α=2.5 for biomass aerosols but only 1 for motor vehicle emissions of light absorbing aerosol. Kirchstetter et al (2004) also provide values of the imaginary part of OC refractive index between 350 and 700nm.
No single study or sample provides values for real, imaginary and wavelength dependent refractive index for OC. The recommendation made here is that SRFA refractive indices at 532nm be used as the anchor point for a wavelength dependent refractive index that retains the dependence of Kirchstetter et al (2004) between 350 and 700nm for the absorption part, but is wavelength independent in the real part (there being a lack of information regarding the wavelength dependence above 532nm) for the visible part of the spectrum. The value at 550nm is more absorbing than that used in HadGEM2, but still substantially less absorbing than HULIS isolated from several samples from different combustion and aerosol conditions. For longer wavelengths still (above 4 micron), Hess et al (1998) wavelength dependence for WASO (water soluble type) is used as in Stier et al (2007). Extreme caution should be attached to the values at longer wavelengths.

Maybe these assumptions need to be updated or questioned, and maybe we should adopt other values for Organic Carbon. However, as mentioned in the manuscript, “ the specification of these parameters is in a parameter file, and can be changed by the user to other values. In the same way, the user can easily introduce more species in the optical treatment for specific studies, e.g. volcanic ashes.”, so it is easy for a user who wants to test the impact of other assumptions to specify other values of the refractive indices.

Fig. 7 : Presumably, the numbers on the right axis of each plot represent the mean value of MFB, MFE and PCOR and therefore should be the same as the read dot in the plot which also represents the mean of each statistic. This does appear to be the case for MFB and MFE, however there seems to be a large discrepancy between the PCOR values listed on the axis and those represented by the red dots on the plots. For instance, the PCOR for O3 summer is listed as 0.69 on the axis but the red dot lies on the 0.6 line. Can you please explain the discrepancy between the two values?

These numbers were actually not explained in the first version of the manuscript. They actually correspond to the overall value of the parameter, e.g. grouping in a single vector all the concentration values for all stations and all time points to obtain a spatiotemporal correlation (respectively, spatiotemporal MFB, etc.). the following sentence has been added to the figure caption :
“the values on the right axis of each panel are the overall value of the considered indicator, i.e. merging all the stations into a single statistical dataset as described in Jacobson (2005)”.

P. 26, l. 3-5 : It could also be argued that 0.5 degree horizontal resolution is insufficient to simulate

urban environments that have a lot of heterogeneity in emission sources. How many of the remaining sites would be classified as urban and rural sites?

It is true that this resolution is not adequate to simulate urban (or industrial) environments. This is why we used EMEP stations for comparison, which are rural background sites. For example, in the reference EMEP publication by Thorseth et al., 2012, *Atmos. Chem. Phys.* States that "The EMEP monitoring sites are located such that significant local influences (local emission sources, local sinks, topographic features, etc.) are minimised. The basic idea is that the data should be representative for a larger region.".
The following sentence has been added : "Stations from the EMEP monitoring sites have been chosen for this study because their location has been selected in order to minimize local influences and be representative of large areas (Thorseth et al., 2012)". (p. 17, l. 17-20)

p. 26, l. 9-11 : Are these statistics for ozone for all hours of the day?

The statistics are for daily averaged values, which was not specified in the first version but is now specified (in the Figure caption and in the text).

p. 26, l. 15-16 : I highly agree with this statement and needs to be addressed more prominently in the manuscript in my opinion. It should be made clear to the reader that the performance of the model at this resolution for anything but background stations should be considered with caution. I would expect considerably different model performance when the resolution of the simulation is increased to a more regional/urban scale.

(I assume that the Reviewer's remark refers to lines 18-19 which are a statement about model's resolution and its possible impact on scores for nitrogen oxydes).
As stated above (in the revised version), the EMEP stations are designed to be representative at least at a regional level, which normally reduces the impact of local factors such as industries or major urban areas and therefore permits comparison with a simulation at 0.5° resolution. However, of course, this is never totally the case and local influences, even though they may be small, can sometimes be present, but by using the EMEP stations that are expert-selected to be representative at regional level we hope to reduce the effect of insufficient model resolution. Detailed reference to studies with higher resolutions is now provided in the Introduction, taken from large international multimodel comparison projects such as AQMEII, Eurodelta (I and III) as well as from urban-scale studies (p. 2, l. 3-49)

p. 26, l. 19 : What emissions specifically are they saying are underestimated?

Unfortunately, the statement in the conclusions of Terrenoire 2015 is not very explicit about this underestimation. The exact statement made in this paper is as follows : "The difficulty for the model in reproducing NO2 concentration is likely to be due to the general underestimation of Nox emissions, especially during the traffic daily peaks, as well as a horizontal resolution that is not high enough to represent correctly the spatial gradients of the emissions over medium and small cities.". The second part of this statement only partly applies to the present study since for the present study only EMEP background measurement sites are retained. We added the words "especially during the traffic daily peaks" to the revised version to make the statement a bit more explicit.

p. 26, l. 22-24 : Can the authors say something about the SO4 performance of the model? Is SO4 underestimated, suggesting issues with the conversion of SO2 to SO4 in the model? It's easy to simply blame the emissions, but more information is needed on the overall performance of the model before

simply blaming emissions for the poor SO2 performance. And what exactly is the issue with the vertical distribution of SO2? Is this suggesting not enough SO2 is being elevated to upper layers in the model? Presumably the primary SO2 sources are energy generating units, which typically emit above layer one. Is this a plume rise issue in the model?

p. 27, l. 1-4 : What about the performance of SO4?

p. 27, l. 5-10 : So the model is overestimating both SO4 and SO2 in the winter? Is SO4 also overestimated in the summer?
(We group the answer to these three remarks)

We agree that it is easy and occasionnally convenient to simply blame the emissions, but is was not our intention here, since we point as a possible error source the vertical profiles for anthropogenic emissions, which are a choice of the model developers, described in Mailler et al. (2013) and Terrenoire et al. (2015). So, what is pointed as a possible error source here is actually a fallback of the model which uses fixed vertical emission profiles (this is now mentioned explicitly, p. 18, l. 30-34). If this is the case, the errors due to this modelling choice would be reflected essentially on SO2 concentrations since SO2 is the species that is the most influenced by industrial stack emissions. We also give more general information on the model's characteristics regarding SO2 ans sulphate, we added more details and references to this part :

"The SO2 shows the largest MFE for both summer (74.5 %) and winter (80.2 %) and quite low correlation in summer (0.20). It shows positive bias in winter: MFB=35.5%. The difficulty of SO23 simulation could be related to the uncertainties in the vertical profiles on emissions, which is a particularly sensitive factor in SO2 simulations since industrial stack emissions represent a substantial part of SO2 emissions (Pirovano et al. 2012, Mailler et al. 2013). While other CTMs have included a plume-in-grid model for subgrid treatment of point emissions depending on the actual meteorological conditions and flux characteristics, this is not the case of the CHIMERE model, which can also limit the performance of the model regarding SO2 concentrations. The conversion of SO2 to sulphate can also be a source of error on SO2 concentrations, as mentioned by Ciarelli (2016) and Bessagnet (2016) who observed very different behaviour of models far from emission sources probably due to the chemical mechanisms. The lower correlation coefficient in summertime is present in all the CTMs examined in Bessagnet (2016)." (p. 18, l. 30-41)

p. 27, l. 5-10 : Are there soil measurement available that could be used to indicate whether or not dust is a major contributor to the bias?

We agree that this statement : "*This might indicate that the dust, whose emissions are very sensitive to the wind speed, contribute to the PM_{10} errors in winter*" is probably too speculative, and we are not aware of routine measurements of mineral dust concentrations that would permit to readily verify this (at least on the EMEP measurement network only nitrate, sulphate and ammonia are measured, to our knowledge). So we removed this statement.

p. 27, l. 9 : These are not actually EPA guidelines. Boylan and Russell published this work due to a lack of clear guidance from the USEPA. Just to be clear.

Thank you for this useful precision. The notion of "EPA guidelines" has therefore been removed from

the text.

p. 27, l. 28 : Important to note that his is well below the stratosphere for most latitudes, so the specification of the the upper boundary conditions becomes very important. What values (i.e. model) was used to provide these boundary values? How well did that model simulate the volcanic plume?

This statement depends on what is meant by “most latitudes”. Actually, if one refers to studies such as Seidel & Randel (2006, J. G. R., their Fig. 3) or Hoinka (1998, M. W. R.), the tropopause will be around 200hPa at 40°S in annual average, higher than that at the low (tropical) latitudes, lower than that at the polar latitudes, reaching ~250-300 hPa. At the latitude at which the plume travels, around 40°S, the top of model is about the same altitude as the tropopause.

However, for the reasons mentioned by the Reviewer, and also to avoid possible “leaks” of particles through model top, the simulation has been redone with model top at 100 hPa, which is higher than both the tropopause and the ash plume (so that the boundary condition at top of model does not need to include the volcanic plume).

As mentioned earlier in the article, the boundary conditions are from a LMDZ-INCA4 climatology.

p. 28, l. 13-15 : What exactly is occurring at the top of the model? This seems to be a very critical component of the global modeling that was performed that was not discussed at all.

Actually, at the top of the model, the concentrations are taken from LMDZ-INCA4 climatology, as for boundary conditions. The boundary condition at top of model is significant essentially for ozone concentrations, which are much stronger in the stratosphere and high troposphere than in the boundary layer. For other trace gases and aerosols, concentrations are very low in the stratosphere compared to their tropospheric concentrations.

p. 29, l. 3-4 : at least to eliminate initial conditions artifacts. What initial conditions were used?

The initial conditions have been taken from a climatology produced by the LMDZ-INCA model, as well as the boundary and top conditions. But this is only for the first time-step of the whole simulation. And to avoid the impact of this uncertainty, all simulations have at least two weeks of spin-up before analysis of the results.

p. 29, l. 2 : My general comment on this analysis is that it represents an evaluation of the meteorology and not the chemistry in CHIMERE. If the simple point of this analysis is that the model can transport a plume across a hemisphere is an at least reasonable fashion, than this analysis is probably sufficient, and should be stated as such. However, the analysis does not provide much faith that CHIMERE can accurately simulate the plume in terms of concentration and composition, which would be a much more useful evaluation.

Fig. 8 : It would be useful to include plots of observed AOD as well for comparison.

It is true that comparison to observational data is missing. However, making a comparison with observational data would require a better input regarding volcanic emissions, which we are not able to do at this point. As an example, the parameter m_{63} quantifying the proportion of fine ash / total ash, is highly uncertain, as well as the total ash quantities emitted, etc. Therefore, we would prefer not to

present comparison to AOD data before this problem is solved, and stay with a qualitative discussion relying on published data analyzing observations to check that the chronology of the plume transport is represented in a realistic way in our simulation.

p. 32, l. 5-11 : I don't find this section to be very enlightening without some comparison to observed value. If the goal is simply to imply that the lidar plots seem to produce reasonable patterns, than it should be made very clear that that is the only goal of creating the plots.

We agree with the Reviewer that this section does not bring much to the study, given that the methodology for calculation of the LIDAR observables is already described earlier, and this plot lacks comparison with actual LIDAR data. Therefore, this subsection has been removed, as we cannot really challenge the idea that it is not very enlightening.

p. 32, l. 17-18 : Based on the limited simulations and analysis performed here, it's difficult to say whether the model can indeed be used to simulate urban to hemispheric scales with reasonable accuracy. No urban or regional scale simulation is presented here.

The reason why urban scale simulations are not presented here is because simulated aurban scale processes is already an existing feature of CHIMERE (as described in the studies of Markakis et al (2015), Valari et al. (2008, 2010) largely cited and described in the present study (p. 2, l. 3-25), while simulating hemispheric scale transport is one of the most significant new features of this version compared to the previous version that was described in Geophys. Model Dev. In 2013. Therefore, the focus is put on this new capability.

CHIMERE-2017 : from urban to hemispheric chemistry-transport modeling

by S. Mailler et al.

Answer to Anonymous Reviewer 2

Please note that the title of the paper has been updated to CHIMERE-2017 instead of CHIMERE-2016 since a new model version has been issued, with only bugfixes from the 2016 version. All the simulations have been redone with this corrected version, which does not bring any change in the discussion since the changes are only small bugfixes.

We would like to thank Reviewer 1 for accepting to review this paper, and for his/her useful remarks.

Below are, in blue, the comments and requests by Reviewer 1, in black our answers, and in green the description of the corresponding changes that have been brought to the Manuscript, when relevant.

General Comments.

The manuscript introduces the new version of the CHIMERE chemical transport model. The text is rather long and requires an English proofreading.

OK, we have performed a proof-reading of the article to try improving the language level and smooth out the differences between the style of the different coauthors. Also, reviewer 1 provided numerous improvements in the quality of language, which were very useful.

Also, providing examples and evaluations with observational data of several new model features will make the paper further compelling.

In our view, this manuscript is a model description manuscript more than model evaluation, since a number of studies already use the CHIMERE model and compare it to observations and to other comparable models, giving to the interested users a detailes view of the performance of the model depending on the species, the resolution, etc. We added some information in this sense in the revised version, including more references to detailed evaluation papers such as Terrenoire (2015) or Bessagnet (2016) . Even though these papers use earlier versions of the model, the model performance in its "classical" regional configuration only evolves smoothly with time even when lots of new developments are included, this is also the case between the described version and earlier versions that have been thoroughly evaluated. Therefore, the focus in this paper is not put on evaluating a strong increase in model performance, which is not the case (the evolution of modelling scores from one version to the next is slow and smooth), but a change in the scope of the model, including more processes, and extending the capabilities in terms of domain size to the hemispheric scale. This precision of the scope of the manuscript can be found in the introduction of the revised paper, p. 2, l. 29-46.

Besides the questions listed below, I recommend to be added to text:
1) A table of variables presented in text,
2) A table describing all physical input variables that are needed from a meteorological model (as WRF or IFS/ECMWF) to drive a simulation with this version of CHIMERE.

For the CHIMERE model, all variables are already cited and described in [Menut et al., 2013].
A table of all the variables that must/can be read from the Meteorological model is now provided in the

revised version (Table 1).

Questions/Comments

Pag 2, abstract, lines 4-10 It seems that there is a mix-up be-tween the words ‘scales’ and ‘domain sizes’ . The authors should refer to scale as the smallest eddy resolved by the model and not mix with the size of the computational grid used to simulated certain phenomena. In this sense, stating that CHIMERE-2016 can be applied at any scale seems to be unsuitable. I invite the authors to rephrase those sentences.

There is maybe a problem of vocabulary in different communities here. For the word “scale” as understood by the Reviewer, we would tend to use “resolution” or “grid spacing”. Due to this remark, we have looked for the use of “scale” as we mean it in the article, finding many example that seem to comfort the use of “scale” to actually mean “domain extension”, as we understand it:
“Hemispheric-scale modelling of Sulphate and Black Carbon and their Direct Radiative Effects” (1998, Book chapter by Alf Kirkevåg and Øyvind Seland)
“Around the world in 17 days - hemispheric-scale transport of forest fire smoke from Russia in May 2003” (Damoah et al., Atmos. Chem. Phys, 2004)
This, and the very widespread use of “regional scale”, “urban scale”, not to mean that the smallest eddy resolved by the model has the scale of a urban area, or a region, but that the whole simulation domain has this size, seems to us the most common way to understand “scale” in this context. See, e.g., “Impact of model grid spacing on regional- and urban- scale air quality predictions of organic aerosol.”, Stroud et al., 2011, Atmos. Chem. Phys., who clearly use “scale” to specify the domain extension, and another notion, “grid spacing”, which is actually equivalent to the smallest resolved eddy - speaking of a chemistry-transport model, whether eddies at this scale are resolved or not depends not on the model itself but on the meteorological data used to force the model. Therefore, as the use of “scale” the way we understand it seems not to be uncommon in our community, and replacing it by “domain size” or an other similar formulation would make many formulations more tedious, we wish to maintain this use of the world scale.

However, to avoid any possible misunderstanding by the readers due to the various possible meaning of the world “scale”, we included the following sentence in the Introduction of the paper in order to (hopefully) lift any ambiguity, and also to bring useful information to the readers of this study:
“The typical resolution (grid-spacing) of the simulation domains range from about 4~km for urban-scale domains to about 50km for regional-scale domains (Markakis et al., 2015, Valari et al., 2008).” (p. 1, l. 49-51)

Pag 2, Introduction State clearly the class of atmospheric-chemistry models which CHIMERE-2016 fits. Is it a coupled online atmospheric-meteorological model? If yes, does it include feedbacks between atmospheric composition and the model dynamics?
Offline model. The following statement has been added :
“CHIMERE-2016 is an offline chemistry-transport model, meaning that it needs to be provided with input meteorological fields, and does not implement any feedback of atmospheric chemistry on atmospheric dynamics.” (p. 2, l. 76-80)

How does it compare with other state-of-the-art models like WRF-Chem and COSMO-ART?

As stated above, CHIMERE-2016 is an offline model, so comparison with WRF-CHEM and COSMO-ART is not relevant. This being said, the question of how CHIMERE compares with similar models is

of interest. For that, the reader is now referred to publications from recent intercomparison exercises in which CHIMERE has participated: AQMEII, Eurodelta I and III, CityDelta etc.. This paragraph is in the introduction of the revised manuscript (p. 2, l. 24-49). The interested reader is referred to these publication who detail the characteristics of each of the participating models for many atmospheric trace components.

Pag 3, line 5 State clearly the means of 'CHIMERE core' . Did you say 'dynamic core'?

The notion of "core" for a Chemistry-transport model is actually not clearly defined, and we suppressed it from the manuscript. We initially meant it as the parallelized part of the model (contrary to preprocessors and I/O which was not parallelized), but this is more internal jargon than a recognized notion. In some other parts of the paper, we also removed this ambiguous notion of "core". This statement has been changed as follows (p. 3, l. 11-16):

"Several technical changes were made in the CHIMERE code to improve code scalability: these changes regard the parallelization of many preprocessors into the parallelized section of the model, along with improvement of the parallelization strategy for some parts of the model that were already parallelized in order to improve code scalability."

Page 3, line 20. The expression master/slaves are more common in this context.

OK, we performed this change throughout the paper.

Page 4, lines 1 – 3. In the new version, clarify if the model output is split into several files (each slave writes its model solution in a particular file) or if each slave writes its own sub-domain but in a single file, which comprises the entire domain.

This precision has been added :

Each slave process writes its own sub-domain into a single output netcdf file common to all slaves (p. 3, l. 67-71).

Page 7, Line 20 Include a brief description of the numerical properties of the advection scheme applied in this chimere version to transport scalars.
These precisions have been added a bit earlier than suggested by the Reviewer, because they did not need to be changed for the new model version. The precisions are brought as follows:

In CHIMERE-2017 as in earlier versions, the user can choose between three different options for horizontal transport schemes, namely the basic upwind scheme, the slope-limited Van Leer scheme (Van Leer 1979), and the Piecewise-parabolic method (Collella and Woodward 1984), all of which are examined in the CHIMERE model in lo2009}. Thes three schemes are designed to estimate the trace species concentration at grid cell interfaces in order to convert the mass flux of total air through cell boundaries into mass fluxes for each of the model species through these boundaries. While the implementation of these schemes has needed no change in building the present model version, the estimate of the atmospheric mass flux between neighbouring model grid cells has been revised by switching to a new coordinate system in order to lift model limitations concerning the geographic poles and the date-change lines. These three schemes are designed to be monotonous (because they include the use of slope-limiting algorithms, except the Upwind scheme which does not need the use of such

algorithm), and mass-conservative because of their flux formulation. (from p. 3, l. 87)

Page 8, section 3.1 The new version aims to simulate tracer transport on continental/hemispheric scales with the model top at 200hPa. How the organized vertical transport of pollutants associated with convective and moist plumes are handled in this configuration?

Vertical transport due to deep convection can be activated by the user. If so, the mass fluxes associated to deep convection are estimated using the Tiedke (1989) scheme, and taking into account the fluxes for each model species in the vertical transport and mixing scheme. This is now mentioned in the revised version.

The following sentence has been added :
"Vertical transport on this mesh can be calculated using either a slope-limited Van Leer scheme (Van Leer 1979) or a upwind scheme, depending on user's choice, also taking into account turbulent mixing and, optionally, deep-convection fluxes, following the Tiedke (1989) formulation as described in Menut et al. (2013)."

Page 16, section 5. Describe the numerical solver of the chemical mechanism applied in this model version.

This was not described in the first version of the Manuscript because the solver is the same as in earlier model version. In the revised version of the manuscript, we added the following text :
"As for earlier model versions, the stiff system of partial differential equations resulting from the chemical mechanism is based on the application of a Gauss–Seidel iteration scheme to the 2-step implicit backward differentiation formula, adapted from the algorithm proposed by [Verwer, 1994] More details on this method can be found in Menut (2013)." (p. 6, l. 74-79)

Page 28, line 12 The emission configuration does not agree with the general observed 'umbrela' shape of the volcanic plume. Page 29, Section 7.4

We agree that the volume and distribution of the volcanic emissions is highly uncertain, in terms of emitted mass, vertical profile and deduced optical properties. But the goal of this new experiment was mainly to evaluate the model ability to correctly reproduce long-range transport with the new configuration of the hemispheric model grid.

The simulation outputs discussion lack comparison with observational data. It would be very instructive for the readers to perceive the fidelity of the model transport and AOD simulations.

It is true that comparison to observational data is missing. However, making a comparison with observational data would require a better input regarding volcanic emissions, which we are not able to do at this point. As an example, the parameter m_{63} quantifying the proportion of fine ash / total ash, is highly uncertain, as well as the total ash quantities emitted, etc.

Page 32, Conclusions. Line 16: Is it true that this version 'has the ability to include all types of emissions'

We agree with the Reviewer that this statement is of course exagerated since some kinds of emissions will always be missing in any model. In the case of CHIMERE, one could mention, for example, the

lightning emission, oceanic DMS emissions, among others. So, we just removed this statement, since the next sentences describe objectively which kinds of emissions have been added since previous model version, which gives more objective and useful information.

~~CHIMERE-2016~~CHIMERE-2017: From urban to hemispheric chemistry-transport modeling

Sylvain Mailler[1,2], Laurent Menut[1], Dmitry Khvorostyanov[1], Myrto Valari[1], Florian Couvidat[3], Guillaume Siour[4], Solène Turquety[1], Régis Briant[1], Paolo Tuccella[1], Bertrand Bessagnet[3], Augustin Colette[3], Laurent Létinois[3], Kostantinos Markakis[1], and Frédérik Meleux[3]

[1]LMD/IPSL, École Polytechnique, Université Paris Saclay, ENS, PSL Research University; Sorbonne Universités, UPMC Univ Paris 06, CNRS, Palaiseau, France
[2]École des Ponts ParisTech, Université Paris-Est, 77455 Champs-sur-Marne, France
[3]INERIS, National Institute for Industrial Environment and Risks, Parc Technologique ALATA, F-60550 Verneuil-en-10 Halatte, France
[4]Laboratoire Interuniversitaire des Systèmes Atmosphériques (LISA), UMR CNRS 7583, Université Paris Est Créteil et Université Paris Diderot, Institut Pierre Simon Laplace, Créteil, France

Correspondence to: Sylvain Mailler (sylvain.mailler@lmd.polytechnique.fr)

Abstract. CHIMERE is a chemistry-transport model ~~initially designed for box-modelling of~~ designed for regional atmospheric composition. ~~In the past decade, it has been converted into a 3D eulerian model that could~~ It can be used at a variety of scales from local to continental domains. However, due to the model design and its historical use as a regional model, major limitations had remained, hampering its use at hemispheric scale, due to the coordinate system used for transport as well as to missing processes that are important in regions outside Europe. Most of these limitations have been removed in the ~~CHIMERE-2016~~ CHIMERE-2017 version, allowing its use in any region of the world and at any scale, from the scale of a single urban area up to hemispheric scale, ~~including or not polar regions~~ with or without polar regions included. Other important improvements have been made in the treatment of the physical processes affecting aerosols and the emissions of mineral dust. From a computational point of view, the parallelization strategy of the model has also been ~~improved~~ updated in order to improve model numerical performance and reduce the code complexity.

The present article describes all these changes. Statistical scores for a model simulation over continental Europe are presented, and a simulation of the circumpolar transport of volcanic ash plume from the Puyehue volcanic eruption in June 2011 in Chile provides a test case for the new model version at hemispheric scale.

1 Introduction

Deterministic chemistry-transport modelling is now widely used for the analysis of pollution events, scenarios and forecast (Monks et al., 2009). Numerous models exist and are used from local to global scale, both for gaseous and aerosols modelling (Simpson et al. (2012); Inness et al. (2013) among many others).

While models were previously dedicated mainly to specific processes, the ~~last~~ latest generation of chemistry-transport models (CTMs) aims at representing the complete set of ~~all~~ processes leading to changes in the atmospheric composition in terms of aerosols and trace gases. For regional air quality in the troposphere, several CTMs are currently developed and are able to include all types of emissions: anthropogenic, biogenic, mineral dust, sea salt, vegetation fires and volcanos. Even though all these emission processes are now included in many CTMs, the emitted species have different chemistry and lifetimes, and models often address some specific applications and thus specific spatial areas. ~~It~~ This was the case of the CHIMERE model, extensively described in Menut et al. (2013a) for its 2013 version. Originally, CHIMERE was designed for urban areas. It was extended later to western Europe, and then to the northern part of Africa by including mineral dust emissions, but was ~~able to run over~~ limited to these areas

only, due to limitations in ~~forcing sources~~ available data (such as the anthropogenic emissions). The typical resolution (grid-spacing) of the simulation domains range from 4 km for urban-scale domains to about 50 km for regional-scale domains Markakis et al. (2015); Valari and Menut (2008).

~~In the new version presented in~~ The CHIMERE model has been used for a long time for studies at the urban to regional scale. Vautard et al. (2007) has used this model within the CityDelta project over four major urban areas in Europe (Berlin, Milan, Paris and Prague), at a horizontal resolution of 5 km. While this resolution is not sufficient to resolve adequately urban-scale phenomena, Valari and Menut (2008) have shown that due to limitations in the accuracy of the input meteorological fields, increasing the horizontal model resolution to values lower than 10 km might actually degrade model performance. The same authors (Valari and Menut, 2010), show that, actually, rather than increasing the model resolution towards kilometric scale, better results can be obtained by downscaling model results to a kilometric resolution representative of urban scale by mixing model outputs with fine scale information on emissions. Recent studies using CHIMERE at urban scale include the work of Markakis et al. (2015), using a set of long-term (10 year) CHIMERE simulations at 4km horizontal resolution for the Paris region, including urban, suburban and rural areas, where the CHIMERE model is used for the present climate but also to test the possible impact of different emission and climate scenarios on air quality in this area. CHIMERE has also been used at continental scale for a long time, including model intercomparison exercises such as AQMEII (Rao et al., 2011; Solazzo et al., 2012b, a), Eurodelta (Schaap et al., 2007) and more recently Eurodelta III Bessagnet et al. (2016). The latter study presents the evaluation of the CHIMERE outputs for the main species of gaseous and particulate atmospheric trace components along with these of six other state-of-the-art models over Europe. The interested reader is therefore referred to Bessagnet et al. (2016) for a detailed comparison of the CHIMERE characteristics and performance compared to other models, and to Terrenoire et al. (2015) for a detailed overview of the CHIMERE performance and scores regarding the concentrations of many gaseous and aerosol species compared to a network of ground measurements over Europe for year 2009). As these studies at continental scale are very recent and dramatic changes in model performance over Europe do not occur from the changes presented here, the present article is not only focused on evaluating the model performance relative to observations but rather on describing the generalization of the model scope to hemispheric scales and the inclusion of new processes. For forecast, the model is daily used for the French PREVAIR system, (Honoré et al., 2008), the COPERNICUS program, (Copernicus, 2017), as well as in many air quality networks.

In this paper, ~~CHIMERE-2016, the~~ the CHIMERE-2017 model version is presented. All new developments made since the CHIMERE-2013 version ~~presented in focus on input databasesand~~ (Menut et al., 2013a) are presented. This mainly consists in an extension of input databases, model grid management~~in order~~, optimization and chemical mechanism. The changes for the grid management are dedicated to build a CTM able to run over a hemispheric ~~domain~~ domains as well as for smaller regions anywhere in the world. These developments required important changes in the model, as well as the improvement of many processes already included in the previous version: the Fast-JX module for realistic evaluation of the photolysis rates has been added and allows the calculation of updated photolysis rates at each physical time step, including the optical effects of clouds and aerosols. The mineral dust emissions have been upgraded in order to estimate fluxes in any region. In addition, this new version has also been an opportunity to update the representation of chemical processes by giving the user the choice to use the SAPRC chemical mechanism, which is more widely used than the MELCHIOR chemical scheme developed for the CHIMERE model~~. In the same line, chlorine~~ (Lattuati, 1997; Menut et al., 2013a). Chlorine chemistry has been included, and the representation of physical processes affecting the aerosols, such as nucleation, coagulation, and wet deposition has been improved, while a scheme for traffic-related resuspension of particulate matter in urbanized areas has been included in the model.

~~CHIMERE being both used for~~ CHIMERE-2017 is an offline chemistry-transport model, meaning that it needs to be provided with input meteorological fields, and does not implement any feedback of atmospheric chemistry on atmospheric dynamics. As the CHIMERE model is used for both analysis and forecast, ~~a~~ particular attention was given to the optimization of computational performance. Numerous improvements were made in the code and are completely transparent for the user: these changes are described in Section 2.

Section 3 presents the changes in the model geometry, including the vertical mesh, as well as changes in the horizontal coordinate system allowing the application of the model to hemispheric scale domains.

Section 4 presents the improvements in the representation of anthropogenic emissions, including the use of the global HTAP emission dataset for anthropogenic emissions, and the improvements in modelling mineral dust emissions.

Section 5 describes the changes in the representation of various physical and chemical processes in the model, such as inclusion of the SAPRC scheme for gaseous chemistry ~~or~~ and inclusion of chlorine chemistry in the model. This section also presents the evolutions in the modelling of the physical processes affecting aerosols, as well as the implementation of the Fast-JX module for radiative transfers. Another major improvement presented in this section is the ability of ~~CHIMERE-2016~~ CHIMERE-2017 to provide LIDAR observables as a model output.

Section 6 presents the application of ~~CHIMERE-2016~~ CHIMERE-2017 to simulations of three winter months and three summer months in a domain covering continental Europe at 50 km resolution, and the scores obtained by the model in comparison with background observations of gaseous and particulate species in this configuration.

Section 7 presents the application of the new model version to the simulation of the eruption of the Puyehue-Cordon Caulle volcano, in the Chilean Andes, in June 2011. This event provides a good testbed for this new version, since the volcanic plume from this volcanic eruption was dense enough to be observed by satellites all along its circumpolar transport around the South Pole.

Finally, Section 8 presents the conclusions of the present study, in terms of applications made possible by this new model version, as well as the outlines for future developments of the CHIMERE model.

2 Optimizations

Several technical changes were made in the CHIMERE code to improve code scalability: these changes regard the ~~inclusion of~~ parallelization of many preprocessors into the ~~CHIMERE core (and therefore their parallelization)~~ parallelized section of the model, along with improvement of the parallelization strategy for some parts of the model that were already parallelized in order to improve code scalability.

2.1 ~~Inclusion~~ Parallelization of preprocessors~~into CHIMERE core~~

Compared to the previous model version, several programs that used to be sequential preprocessors executed before ~~running the model core~~ the CHIMERE run itself have now been parallelized and included into the ~~model core~~main CHIMERE executable. This is the case of the interpolation and treatment of the input meteorological fields. In the new model version, these fields are read and processed at each hourly time step (instead of being processed once and for all in a sequential way at the beginning of the run). This new design has no impact on the model outputs but has two advantages:

1. It allows a reduction of computation time by parallelization of this calculation step

2. It enables the possibility to develop an online coupled version of the model, in which case the meteorological fields would not be available before the beginning of the simulation.

Note that this ~~“~~"real-time~~”~~ " processing of the meteorological fields is only available for users who use meteorological fields from WRF. For users of other sources of meteorological data such as ECMWF products, offline meteorological preprocessors are still provided with the model. Another important point is that even though the processing of meteorological input has been changed as described here, the present version does not take into account any radiative or microphysical feedback of atmospheric chemistry on meteorology.

Table 1 lists the variables that can be read by CHIMERE from the outputs of the meteorological model, separating the variables that are mandatory from the optional ones.

2.2 Improvement of the parallelization

In 2006, the ~~CHIMERE core~~ main CHIMERE loop was parallelized using a master/~~worker~~ slave pattern. A cartesian division of the simulation domain into several sub-domains is done, each sub-domain being attributed to one ~~worker~~ slave process. Each ~~worker~~ slave performs the model integration in its own geographical sub-domain as well as boundary condition exchanges with its neighbours in order to permit transport from one ~~worker~~ slave to the next. In addition, in former CHIMERE versions, a master process was needed in order to gather and scatter data from the ~~workers~~ various slave processes that performed the actual gridded calculations, and to perform initializations and file input/output.

The use of a master process limited the efficiency of the parallelized code, since the master process did not perform any computation except gathering and scattering the data to and from the ~~workers~~slaves, and that it totally centralized the input and output tasks, a bottleneck effect which limited the gains realized by parallelization, particularly when the simulation domains were very large and split between many ~~workers~~slaves.

Therefore, in the ~~CHIMERE-2016~~ CHIMERE-2017 version, this master process has been removed: using the parallel input/output routines of the Parallel-Netcdf library (Li et al., 2003), each ~~worker~~ slave process now reads the netcdf input files and writes the output data for its own sub-domain into a single output netcdf file common to all slaves, removing the bottleneck effect due to the centralization of input/output tasks.

This induces some major simplifications of CHIMERE code, including reduction of inter-process communications related to the parallelization of the input/output processes, which were performed in a central way by the master process in previous model version.

3 Model geometry

Major changes have been implemented in ~~CHIMERE-2016~~ CHIMERE-2017 compared to earlier CHIMERE versions, opening the possibility to perform simulations in domains including the pole.

Historically, CHIMERE ~~has been~~ was first designed as a box model for the region of Paris (Menut et al., 2000).

CHIMERE name	Variable	Dimension	Units
Mandatory Variables			
lon	longitude of gridpoints	2D	degrees_east
lat	latitude of gridpoints	2D	degrees_north
tem2	2m Temperature	2D	K
soim	Soil moisture	2D	m^3/m^3
rh2m	2m Relative humidity	2D	0-1
lspc	Large-scale Precipitation	2D	$kg/m^2/hour$
copc	Convective Precipitation	2D	$kg/m^2/hour$
temp	Temperature	3D	K
cliq	Cloud liquid water content (excluding rain water)	3D	Kg/Kg
sphu	Specific humidity	3D	kg/kg
pres	Pressure	3D	Pa
alti	Altitude of half layer	3D	m
winz	Zonal component of the wind	3D	m/s
winm	Meridional component of the wind	3D	m/s
swrd	Short Wave Radiation	2D	W/m^2
Optional Variables			
lwrd	Long Wave Radiation	2D	W/m^2
sshf	Surface sensible heat flux	2D	W/m^2
slhf	Surface latent heat flux	2D	W/m^2
usta	Friction velocity	2D	m/s
hght	Boundary layer height	2D	m
weas	Water equivalent accumulate snow	2D	kg/m^2
snowh	Snow height	2D	m
seaice	Sea-ice ratio	2D	*n/a*
psfc	Surface pressure	2D	Pa
rain	rain water content	3D	Kg/Kg
cice	ice content	3D	Kg/Kg

Table 1. *Mandatory and optional variables obtained from meteorological input data. If the optional variables are not provided by the raw meteorological model, there are diagnosed during the simulation.*

Rapidly, it has been transformed into a cartesian model on curvilinear Arakawa C-grids (Arakawa and Lamb (1977), see Fig. 1). However, the formulation of the transport scheme on these curvilinear grids up to CHIMERE-2014b was still based on a lat-lon formulation, which implied the impossibility to include poles in the domain. In CHIMERE-2017 as in earlier versions, the user can choose between three different options for horizontal transport schemes, namely the basic upwind scheme, the slope-limited Van Leer scheme (Van Leer, 1979), and the Piecewise-parabolic method (Colella and Woodward, 1984), all of which are examined in the CHIMERE model in Vuolo et al. (2009). These three schemes are designed to estimate the trace species concentration at grid cell interfaces in order to convert the mass flux of total air through cell boundaries into mass fluxes for each of the model species through these boundaries. While the implementation of these schemes has needed no change in building the present model version, the estimate of the atmospheric mass flux between neighbouring model grid cells has been revised by switching to a new coordinate system in order to lift model limitations concerning the geographic poles and the date-change lines. These three schemes are designed to be monotonous (because they include the use of slope-limiting algorithms, except the Upwind scheme which does not need the use of such algorithm), and mass-conservative because of their flux formulation.

~~These restrictions have been removed in CHIMERE-2016~~ This has been achieved by switching from a representation of the grid points in a spherical ~~coordinate systems~~lat-lon coordinate system, singular at the pole, to a 3d cartesian coordinate system, which has no singularity~~at the poles~~. In the former CHIMERE versions the grid centers were represented by their geographical coordinates $\left(\lambda^{ij}, \phi^{ij}\right)$, and the wind vectors by their projection on the local frame $\left(\mathbf{u}_\lambda, \mathbf{u}_\phi\right)$ (Fig. 2). In the present version, the points are represented by their cartesian coordinates in the frame centered at the Earth center and with unit vectors $\left(\mathbf{u}_1, \mathbf{u}_2, \mathbf{u}_3\right)$, and the wind vectors are represented by their projections on these unit vectors.

This change in the internal representation of spherical geometry has only a small impact on the simulated values, in the sense that it corrects some geometrical errors that appeared due to the assumptions made in the old coordinate system, but these differences have been found to be of very

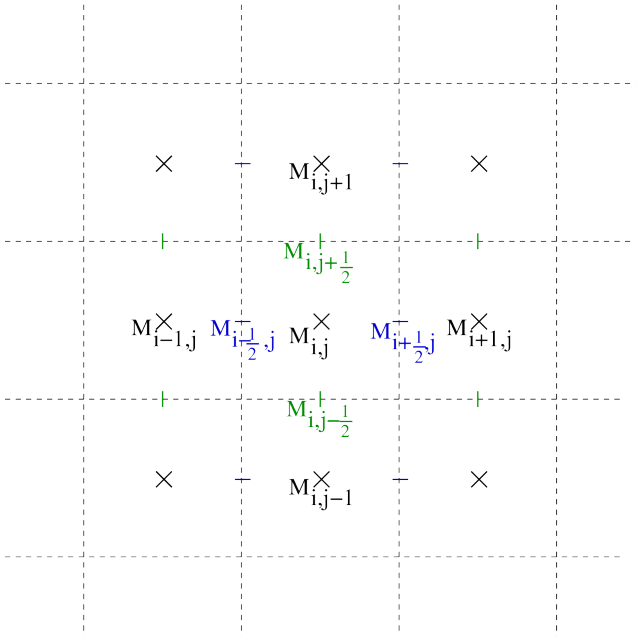

Figure 1. *Centered (black) and staggered (blue and green) grid points in the Arakawa C-grid.*

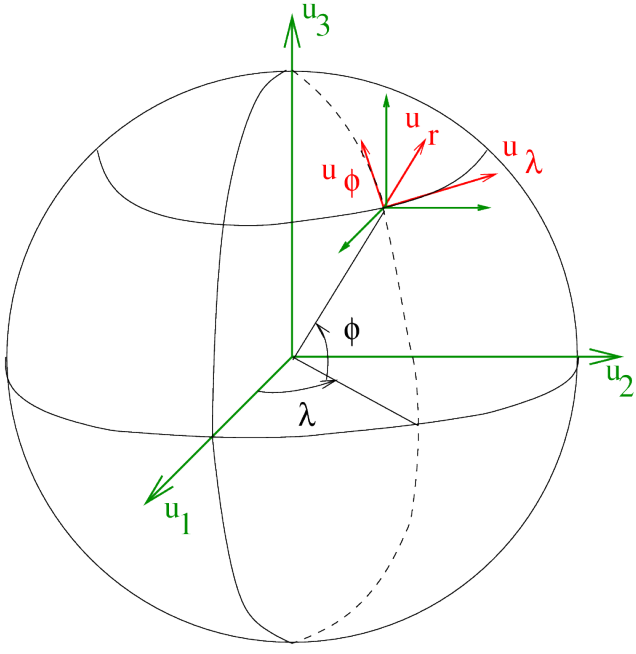

Figure 2. *Cartesian and spherical frames for the representation of point coordinates and speed vectors*

small amplitude, except in the vicinity of the pole where distorsions due to the lat-lon system ~~became~~ become critical. The new coordinate system allows domains that include the pole, without the need for any particular filtering. This strategy ~~permits to build~~ allows the creation of regional domains from local to hemispheric scale anywhere on the globe, including one pole or even~~both of them~~, which opens possible application of ~~CHIMERE-2016~~ CHIMERE-2017 for studies in the polar areas, including circumpolar transport of polluted air masses, as will be shown in Section 7. An example grid on which ~~CHIMERE-2016~~ CHIMERE-2017 can be run is shown on Fig. 3. This grid is a polar stereographic grid centered at the north pole, entirely covering the northern hemisphere, and with the four corners of the domains extending slightly into the southern hemisphere (as far south as 19.47°S). With this projection and this number of points, the horizontal model resolution varies from 140x140 km^2 at the pole to 70x70 km^2 at the Equator.

In this new coordinate system, the transport is calculated as follows. First, the coordinates of every grid center M^{ij} are converted from their geographical coordinates $\left(\lambda^{ij},\phi^{ij}\right)$ to cartesian coordinates $\left(x_1^{ij},x_2^{ij},x_3^{ij}\right)$ on a unit sphere as follows:

$$\left\{\begin{array}{lcl} x_1^{ij} &=& \cos\phi^{ij}\cos\lambda^{ij} \\ x_2^{ij} &=& \cos\phi^{ij}\sin\lambda^{ij} \\ x_3^{ij} &=& \sin\phi^{ij} \end{array}\right. . \quad (1)$$

The horizontal wind vector $\mathbf{U}^{ij}$ at the grid center is initially represented by the two classical wind components: $\mathbf{U}^{ij}=u^{ij}\cdot\mathbf{u}_\lambda+v^{ij}\cdot\mathbf{u}_\phi$ where the zonal and meridional wind components u^{ij} and v^{ij} are obtained from the meteorological inputs. Since this representation splitting the horizontal wind into a zonal and a meridional component is singular at the geographical poles, before performing the transport operations, the horizontal wind is split into its three components on the cartesian frame $(\mathrm{u}_1,\mathrm{u}_2,\mathrm{u}_3)$ using the following formulae for projecting the wind on the cartesian frame $(\mathbf{u}_1,\mathbf{u}_2,\mathbf{u}_3)$:

$$U_1^{ij}=-\sin\lambda u^{ij}-\sin\phi\cos\lambda v^{ij} \qquad \left\{\begin{array}{lcl} U_1^{ij} &=& -\sin\lambda u^{ij}-\sin\phi\cos\lambda v^{ij} \\ U_2^{ij} &=& \cos\lambda u^{ij}+\sin\phi\sin\lambda v^{ij} \\ U_3^{ij} &=& \cos\phi v^{ij} \end{array}\right. \quad (2)$$

$$U_2^{ij}=\cos\lambda u^{ij}+\sin\phi\sin\lambda v^{ij}$$

$$U_3^{ij}=\cos\phi v^{ij}$$

Once the cartesian coordinates of the grid centers $\left(x_1^{ij},x_2^{ij},x_3^{ij}\right)$ and of the wind-speed vectors $\left(U_1^{ij},U_2^{ij},U_3^{ij}\right)$ are computed at the grid centers, it is easy to obtain the values of the speed vectors at the staggered cells (Fig. 1) with the following formulae:

$$U_k^{i+\frac{1}{2},j}=\frac{U_k^{ij}+U_k^{i+1,j}}{2}\,(k=1,2,3)$$

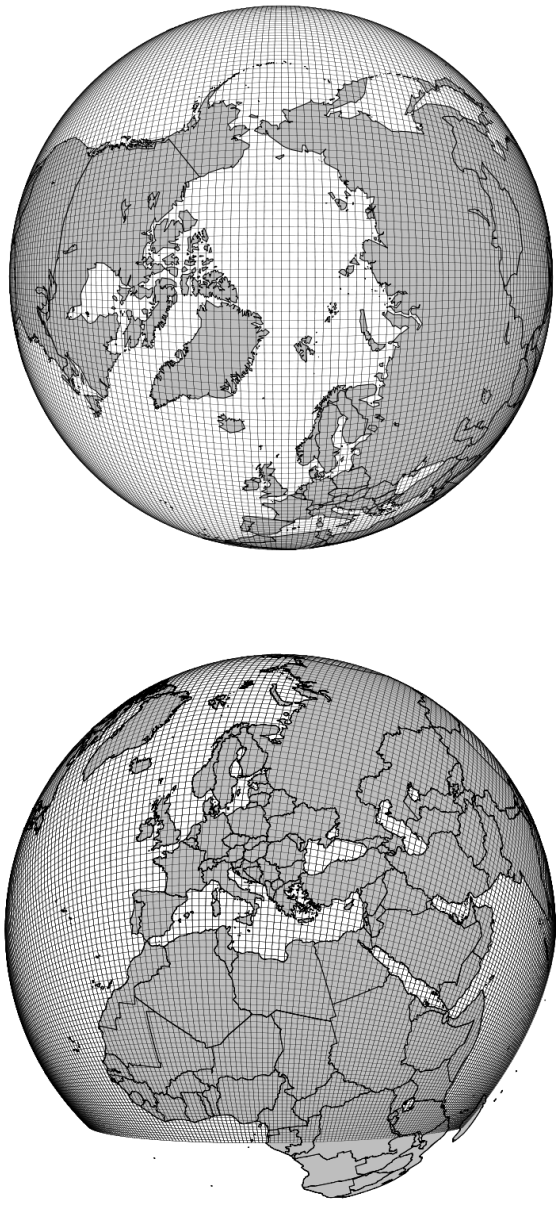

Figure 3. *Model grid generated for the northern hemisphere with 180x180 points in polar stereographic projection, viewed from the top (upper panel) and from the side (lower panel).*

$$U_k^{i,j+\frac{1}{2}} = \frac{U_k^{ij} + U_k^{i,j+1}}{2} \, (k = 1,2,3)$$

$$\begin{cases} U_k^{i+\frac{1}{2},j} = \frac{U_k^{ij} + U_k^{i+1,j}}{2} \, (k = 1,2,3) \\ U_k^{i,j+\frac{1}{2}} = \frac{U_k^{ij} + U_k^{i,j+1}}{2} \, (k = 1,2,3) \end{cases} \quad (3)$$

This new formulation with the use of cartesian coordinates instead of geographical latitude-longitude coordinates for the transport of pollutants removes the constraints that prevented the use of CHIMERE on domains including a geographic pole and/or a date-change line. This new formulation has been tested on the case of the eruption of the Puyehue volcano, in June 2011, a case during which the ash plume from the volcano went around the south pole through the southern Atlantic, Pacific and Indian Oceans back to South-America after 15 days (Section 7). This case is a perfect testbed for the ability of the model so simulate circumpolar movements, and evaluate its ability to represent the location of an aerosol plume after several days/weeks of travel.

3.1 Vertical mesh calculation

The vertical discretization of CHIMERE needs to obey twofold requirements. First, as it has been the case since the beginning of the development of the model, the vertical mesh needs to be very refined in the lowest atmospheric layers because these layers are critical for the modelling of boundary layer contamination, particularly in urban areas, but also in marine areas ~~in order to model correctly the~~ with sea-salt emissions, and in arid areas ~~, for~~ with mineral dust emissions. On the other hand, the CHIMERE model is now used not only for studies at urban/regional scale, but also for studies at continental and, from the present version, hemispheric scale. Therefore, a relatively fine vertical resolution is also needed in the free troposphere to be able to simulate the transport of trace gases and aerosols over large distances avoiding excessive numerical diffusion. Therefore, due to ~~this twofold requirement, the CHIMERE-2016~~ these two requirements, the CHIMERE-2017 vertical mesh is defined as described below.

Regarding the vertical discretization, the user has three degrees of freedom:

- the thickness of the first layer. The user can fix the top of the first model layer, by setting the top of the first model layer in sigma coordinates : $\sigma_1 = 0.997$ corresponds to a thickness of about 3 hPa for the first model layer, about 30 m.
- The number of layers, typically from 8 to 20 layers for the most common configurations of the model.
- The pressure of the top of the model, p_{top}, ~~typically~~ can be freely set by the user with typical values from 500 hPa for studies at urban/regional scales to ~~200~~ 100 hPa for continental/hemispheric scale studies.

From these user-defined parameters, a preprocessing tool calculates a vertical grid as follows:

- From the surface to 800 hPa, the layer thickness (in hPa) increases exponentially

– From 800 hPa to the top of model, the layers are evenly distributed, with equal thickness for each layer.

This procedure outputs the pressure of the level tops, for a reference surface pressure p_{ref} of 1000 hPa. However, the model levels need to adapt themselves to the variations of the surface pressure, essentially due to orography. This is ensured by scaling linearly the pressure levels between the surface pressure and the pressure at the top of model, p_{top}, producing two sequences of coefficients a_i and b_i, such that the pressure at the top of level i is given by $p_i = a_i p_{ref} + b_i p_{surf}$. These coefficients are given by the following expressions:

$$a_i = \frac{p_{top}\,(p_1 - p_i)}{p_{ref}\,(p_1 - p_{top})} \tag{4}$$

$$b_i = \frac{p_1\,(p_i - p_{top})}{p_{ref}\,(p_1 - p_{top})} \tag{5}$$

The linear scaling of the pressure levels by these two sequences of coefficients ensures that the pressure levels never cross each other, and that their relative thickness stays the same even above high topography, as shown in Fig. 4. Vertical transport on this mesh can be calculated using either a slope-limited Van Leer scheme (Van Leer, 1979) or a upwind scheme, depending on User's choice, also taking into account turbulent mixing and, optionnally, deep-convection fluxes, following the Tiedtke (1989) formulation.

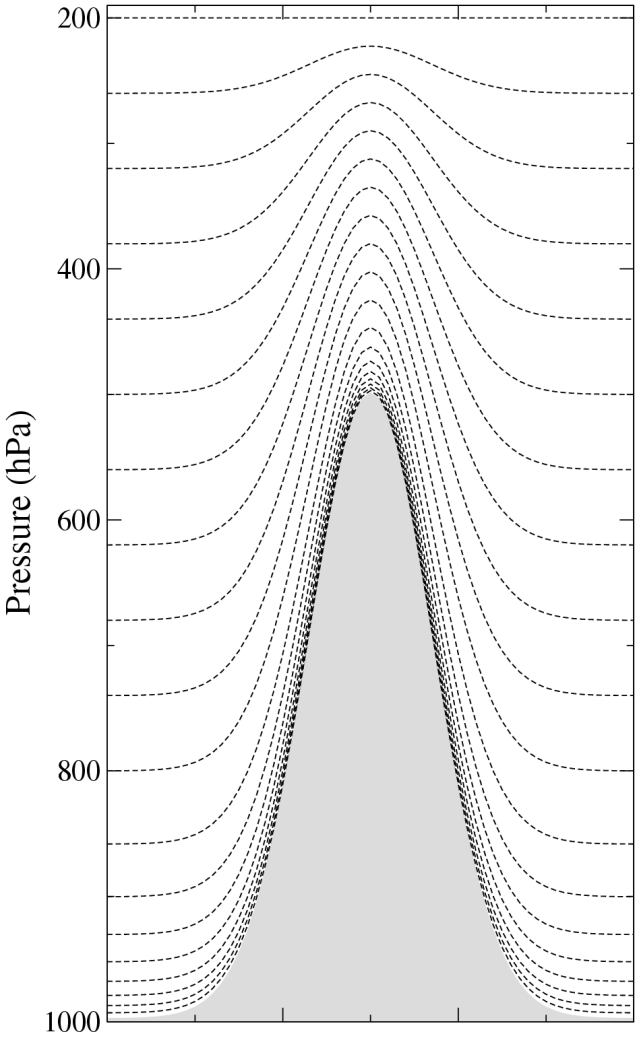

Figure 4. *Model pressure levels with 20 vertical levels, thickness of the first model layer is 3 hPa, top of model set at 200 hPa. Pressure levels are represented across an idealized mountain ~~which~~ with a top ~~is located~~ at 500 hPa.*

4 Emissions

4.1 The anthropogenic emissions

4.1.1 Overall description

CHIMERE needs to be forced at least by input meteorological fields, and by anthropogenic emissions. A preprocessor for anthropogenic emissions, named *emisurf*, is provided to the users. This preprocessor was historically developed for the downscaling and reformatting of the raw emissions from the EMEP emission inventory at 50 km resolution, but can be adapted by users to any other raw dataset they need to use. The main steps for this are described in Menut et al. (2012):

– A first step projects the annual masses from the "raw" EMEP grid to the CHIMERE grid. The spatial emission distribution from the EMEP grid to the CHIMERE grid is performed using proxys like population density, as described by Figs. 5a-d. Proxies used by *emisurf* for this process include land use data (either GLCF, USGS or GlobCover), large point source database (such as the EPER database for Europe), etc.

– Second, monthly, weekly and hourly profiles are prescribed to convert annual totals to hourly fluxes used as input for CHIMERE. These factors are derived largely from data provided by the University of Stuttgart (IER) as part of the GENEMIS project (Friedrich and Reis, 2004), and are available as data files from the EMEP model website, www.emep.int.

– A last step consists in converting the species available in the raw data into the model species. Generally, a minimum of seven species are available: CO, SO_x, NO_x, NH_3, NMVOC, $PM_{2.5}$ and PM_{coarse} (difference between PM_{10} and $PM_{2.5}$). In CHIMERE, depending on the chemical scheme, about 30 species are emitted. NO_x is split into NO, NO_2 and HONO. Usually, 5 to 10 % is assigned for NO_2 emissions for all sectors, except for traffic emissions where a 20% should assigned to NO_2 for modern fleet (post 2010). For NMVOC, the VOC

data used are derived from the detailed United Kingdom speciation given in Passant (2002). For SO_x, 99% is assigned to SO_2 and 1% for primary sulphate to account for very fast and local sulphate production. The lumping procedure accounts for the reactivity of VOC species following Middleton et al. (1990).

The vertical distributions were originally based upon plume-rise calculations performed for different types of emission ~~source~~ sources which are thought typical for different emission categories, under a range of stability conditions (Vidic, 2002), but have since been simplified and adjusted to reflect the more recent findings of (Bieser et al., 2011). The main changes have been for the residential sector where now 100% of the emissions are placed in the lowest ~~model layer~~20 m of the atmosphere, reflecting the large dominance of domestic combustion for this emission category. Also, emissions from large combustion facilities in SNAP sectors 1 and 4 corresponding to large industrial facilities burning fossil fuels are attributed to lower layers than in Vidic (2002), resulting in enhanced concentrations of primary species such as NO_x and SO_x in the boundary layer, in better agreement with routine surface observations, as discussed in ~~.~~ Mailler et al. (2013). The vertical distribution profiles that are used for each SNAP ("Selected Nomenclature for Air Pollutants") sector are constant profiles depending only on the SNAP sector, and are presented in Terrenoire et al. (2015)

4.1.2 Recent changes

The main recent changes have been focused on the use of proxies to better reallocate in space the raw emissions. This specialization can be performed from the raw gridded data or directly from the annual country totals (Terrenoire et al., 2015).

The European Pollutant Release and Transfer Register (E-PRTR) data are used to precisely place the emissions from the main industrial sources. E-PRTR is the Europe-wide register that provides easily accessible key environmental data from industrial facilities in European Union Member States and in Iceland, Liechtenstein, Norway, Serbia and Switzerland.

~~For~~ To treat road traffic emissions ~~, a new spatial proxy was developed based on the correlation between the French bottom-up emission inventory~~ at the European scale, a spatial proxy to distribute the annual country emissions has been developed. This proxy provides a unitless value for a given cell at 1km resolution ~~and different spatial databases . This work was extrapolated over the european domain. It used the~~ over Europe. It is built by crossing several databases (population, land cover data, roads, etc...), it consists of a linear regression of several parameters like population density, length of road, and surface of urban areas in a given fine grid cell. The regression coefficients are calculated over France thanks to the use of the French high resolution bottom-up inventory and applied everywhere over Europe, Figure 6.

For the extrapolation at the European level, it uses the best source of information among the following proxies: CORINE land cover (from the European Environment Agency), road data of the ETISplus European project (European Transport policy Information System) for 2010 over Europe. ETISplus combines data, analytical modelling with maps (GIS), a single online interface for accessing the data. Default European GIS road data from EuroglobalMap, default worldwide GIS road data from Natural Earth data~~(http://www.naturalearthdata.com/)~~[1], and population database by Gallego (2010) over Europe and data from Center for International Earth Science Information Network (CIESIN) for the rest of the world. All of these data were not available on the whole domain. Therefore, three tiers of information were defined to cover all countries with different levels of confidence:

- Countries covered by all the data: Iceland, Norway, Turkey, Bosnia Herzegovinia, Serbia, Montenegro, Kosovo, Macedonia, Albania and all the EU28 except Greece.
- Countries without CLC coverage but with ETIS or EuroglobalMap datas: Belarus, Ukraine, Moldavia and Greece
- Other countries are only covered by the world roadmap and population data.

For shipping emissions (SNAP 8), a proxy was developed using an inventory of shipping routes obtained from the US National Center for Ecological Analysis and Synthesis (NCEAS). ~~An inventory was~~ A database of pressure on marine ecosystems has been developed for the year 2008 by Halpern et al. (2015) but the dataset remains non-exhaustive, the data being collected only on voluntary vessels.

4.2 Mineral dust emissions

Mineral dust modelling is an important process for climate ~~processes~~ evolution understanding but also for air quality regional modelling. For many regions over the world, it becomes necessary to manage air pollution knowing the relative part of anthropogenic and natural contributions. For this, even over small regions, it is important to have the same level of knowledge on mineral dust emissions as for anthopogenic or biogenic emissions. In this new model version, many improvements were done for mineral dust emissions. They are related to input databases, the emission schemes themselves and additional options to better take into account the impact of meteorological conditions on emissions.

[1] http://www.naturalearthdata.com/

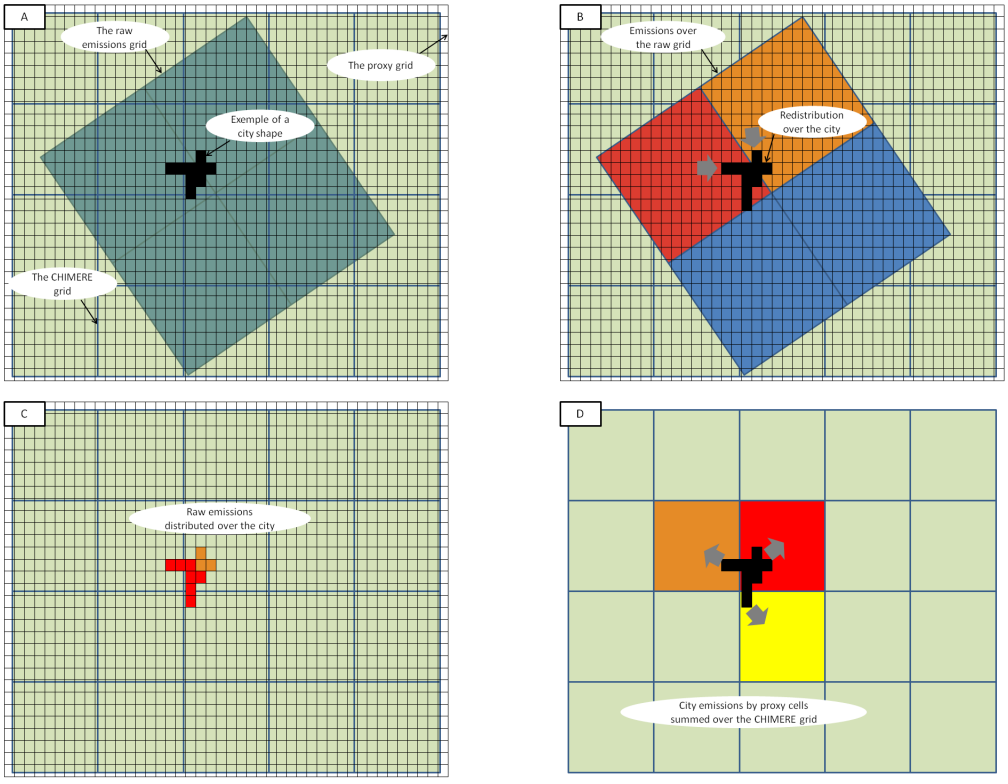

Figure 5. *Downscaling strategy for the anthropogenic emissions*

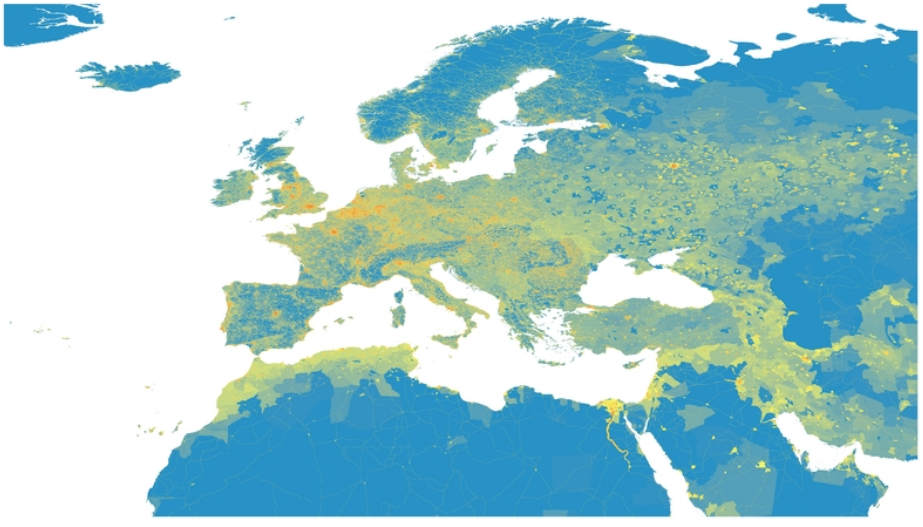

Figure 6. *Map of the unitless value calculated for the traffic emission proxy: low (blue) to high (red) values*

4.2.1 Soil, landuse and roughness length

For the calculation of mineral dust emissions, several variables have to be known: landuse, soil characteristics, aeolian

roughness length and erodibility. Originally, CHIMERE used a database limited to North Africa and the Arabian peninsula. For simulations over Africa or Europe, this spatially limited database was considered adequate, Sahara being the major source in this region. But for this new ~~CHIMERE-2016~~ CHIMERE-2017 version, the goal is to enable calculations of mineral dust emissions anywhere in the world. It is then necessary to change all required databases and to move to global databases. A large part of this change was already done in Menut et al. (2013b) for landuse, soil and roughness length. The soil and landuse used are now those from NCAR USGS landuse dataset (Homer et al., 2004) and STATSGO-FAO soil dataset (Wolock, 1994). The roughness length is estimated using the global 6km horizontal resolution ~~GARLAP (~~"Global Aeolian Roughness Lengths from ASCAT and PARASOL~~)~~" dataset (Prigent et al., 2012).

In addition to these changes, the possibility to evaluate the soil erodibility based on satellite data was added. In the previous versions, the erodibility was based on the landuse database: cropland, grassland, shrubland and barren or sparsely vegetated areas were considered as erodible. In this case, constant percentages are applied for each landuse. While this possibility is maintained in ~~CHIMERE-2016~~CHIMERE-2017, a new option uses the global erodibility dataset derived from MODIS, as presented in Grini et al. (2005), and already included in CHIMERE and used, as described by Beegum et al. (2016). A mix between the two options was also added, making possible to use MODIS only over desert areas and the USGS landuses categories elsewhere.

4.2.2 The Kok's scheme for mineral dust emissions

In this model version, the Kok mineral dust emissions parameterization is proposed, in addition to the ~~and~~ Marticorena and Bergametti (1995) and Alfaro and Gomes (2001) schemes.

The Kok scheme is fully described in the articles ~~, and~~ Kok et al. (2014b), Kok et al. (2014a) and Mahowald et al. (2014). The vertical dust flux is calculated as:

$$F_d = C_d\, f_{bare}\, f_{clay}\, \frac{\rho_a \left(u_*^2 - u_{*t}^2\right)}{u_{*st}} \left(\frac{u_*}{u_{*t}}\right) C_\alpha \frac{u_{*st} - u_{*st0}}{u_{*st0}} \tag{6}$$

where f_{bare} and f_{clay} represent the relative fraction of bare soil and clay soil content, respectively. The flux is calculated only if $u_* > u_{*t}$. The threshold friction velocity, u_{*t}, is calculated using the ~~or the~~ Iversen and White (1982) or the Shao and Lu (2000) scheme (a user's choice). The corresponding u_{*st} is this friction velocity but for a standard atmospheric density ρ_{a0}=1.225 kg m^{-3}:

$$u_{*st} = u_{*t} \sqrt{\frac{\rho_a}{\rho_{a0}}} \tag{7}$$

u_{*st0} represents u_{*st} for an optimally erodible soil and was chosen as u_{*st0}=0.16 m s^{-1} in Kok et al. (2014b). The dimensionless coefficient C_α is chosen as C_α=2.7.

The dust emission coefficient C_d represents the soil erodibily as:

$$C_d = C_{d0} \exp\left(-C_e \frac{u_{*st} - u_{*st0}}{u_{*st0}}\right) \tag{8}$$

with the constant dimensionless coefficients C_e=2.0 and C_{d0}=4.4 10^{-5}.

The vertical dust flux is integrated over the whole size distribution. This flux is thus redistributed into the model dust size distribution as:

$$\frac{\mathrm{d}V_d}{\mathrm{dln}D_d} = \frac{D_d}{c_v}\left[1 + \mathrm{erf}\left(\frac{ln(D_d/D_s)}{\sqrt{2}\mathrm{ln}\sigma_s}\right)\right] \exp\left[-\left(\frac{D_d}{\lambda}\right)^3\right] \tag{9}$$

with V_d the volume of mineral dust aerosols for each mean mass median diameter D_d, C_v=12.62 μm, σ_s=3.0, D_s=3.4 μm and λ=12.0 μm.

4.2.3 Impact of vegetation ~~, humidity and rain~~ on dust emissions

~~As possible emissionsareas are extended, it is necessary to revise the potential impact of vegetation, soil humidity and rain on emissions.~~

The vegetation evolves during the year and this variability will impact the mineral dust emissions. Contrarily to the previous model version, more focused on Saharan areas, this version is able to model mineral dust all around the world. For example in areas such as the Sahelian region or Europe, mineral dust are observed but are very dependent on the vegetation variability. To take into account ~~the impact of vegetation, representing the variations of the aeolian roughness length becomes necessary for simulations areas with a significant annual cycle of the vegetation. In this model version, the monthly~~ this variability, the vegetation fraction is ~~used to ponderate the emission flux when vegetation grows~~diagnosed from the USGS 30s resolution database and acts as a limiter to the erodibility factor.

~~It is also necessary to take into account the~~

4.2.4 Impact of rain on dust emissions

The possibility to inhibit or moderate dust erosion in case of rainfall ~~. This is done in the following two ways. First, during~~ was improved in this model version. In the previous model versions, the complete inhibition of mineral dust emissions during a rainfall event was already considered. In this version, a ~~precipitation event~~ "rain memory function" was added in order to take into account the possible crustation of the soil (Ishizuka et al., 2008) and thus the fact that emissions are also reduced after a rainfall event, even if it is finished. For this calculation, ~~the mineral dust emissions are completely cancelled. Second, dust erosion not reinitiated immediately after a precipitation event, the soil being potentially crusted . To take into account this latter effect,~~ a simple ~~function describing a~~ factor f_p is applied to moderate the dust emissions fluxes when a precipitation is diagnosed and during the next hours as:

$$f_p = E_{dust}\left(1 - \exp\left(\frac{-2\pi\,\Delta t_p}{\tau}\right)\right) \tag{10}$$

with Δt_p the time since the last precipitation event and τ the period after which the surface mineral dust fluxes E_{dust} is fully taken into account, considering that the inhibiting effect of precipitation is finished. For this study, Δt_p is in hours and τ=12. This function is displayed in Fig. 7.

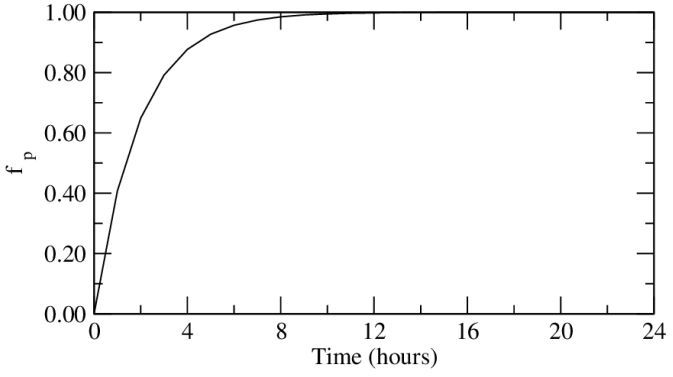

Figure 7. *Function defined to moderate the mineral dust emissions fluxes after a precipitation event.*

4.2.5 Impact of soil humidity on dust emissions

In the absence of precipitation, the soil moisture may also inhibit mineral dust erosion. This effect is taken into account using the Fecan et al. (1999) parameterization. This scheme considers that soil moisture will increase the threshold friction velocity, u_*^T, used to determine if erosion occurs or not. To distinguish between soil conditions, the dry and wet threshold friction velocities are defined, and noted u_*^{Td} and u_*^{Tw}, respectively. u_*^{Tw} is estimated as a possible increase of u_*^{Td} depending on the modelled gravimetric soil moisture w (in kg.kg^{-1}):

$$u_*^{Tw} = f(w)\,u_*^{Td} \tag{11}$$

In the model, the dry treshold friction velocity, u_*^{Td} is calculated following the scheme of Shao and Lu (2000). The $f(w)$ factor is estimated as:

$$\begin{cases} f(w) = 1 & \text{for } w < w' \\ f(w) = \left[1 + \mathrm{A}\,(w - w')^{\mathrm{b}'}\right]^{0.5} & \text{for } w > w' \end{cases} \tag{12}$$

where A and b′ are constants to estimate, and w' corresponds to the minimum soil moisture from which the threshold velocity increases. The values of A, b' and w' are dependent on the soil texture. For A and b', the values are fixed to A=1.21 and b'=0.68. Using measurements data, Fecan et al. (1999) showed that the value of w' is mainly dependent on the clay content of the soil and proposed the following fit:

$$w' = 0.0014(\%clay)^2 + 0.17(\%clay) \tag{13}$$

Note that in equation 12, the gravimetric soil moisture w has to be expressed in %, w' being in % in equation 13 (a conversion is done from kg/kg to %).

4.3 ~~Primary particulate matter~~ Traffic-related resuspension

The resuspension process is important for particulate matter and may induce a large increase of the emission flux in case of dry soils, for locations where traffic and industries produce particles that may be deposited on the ground and therefore become available for resuspension. In this model version, the resuspension flux is active only for cells containing an urbanized surface. The flux is affected to Primary Particulate Matter (PPM) emissions only and thus considered in the model as an anthropogenic process.

The formulation is derived from the bulk formulation originally proposed by Loosmore (2003). The resuspension rate λ, in s^{-1}, is expressed as:

$$\lambda = 0.01\frac{u_*^{1.43}}{\tau^{1.03}} \tag{14}$$

where τ is the time after the start of resuspension. This time is taken into account considering that particles are first deposited then resuspended. The detail of the processes leading to resuspension are essentially unknown, and we assume here that the available concentration of particulate matter depends only on the wetness of the surface. In this empirical view, the resuspension flux is assumed to be:

$$F = P\,f(w)\,u_*^{1.43} \tag{15}$$

where $f(w)$ is a function of the soil water content and P is a constant tuned in order to approximately close the PM_{10} mass budget over Europe estimated in Vautard et al. (2005). It was found to give a correct amount of additionnal PM_{10}. In this model version, P is approximated as $P = 4.72\,10^{-2}\,\mu g m^{-2} s^{-1}$ if we consider European mean conditions with a soil water content of 25% and a friction velocity of u_*=0.5 m.s^{-1}.

The soil water function $f(w)$ is estimated as:

$$f(w) = \frac{w_s - w}{w_s - w_t} \tag{16}$$

where $w_t = 0.1$ is a soil moisture threshold below which resuspension is activated, and w_s is the maximum of soil moisture ponderated by the ratio of water and soil densities, as:

$$w_s = w_{max} \frac{D_{water}}{D_{soil}} \tag{17}$$

with $w_{max} = 0.3$ is a constant value representing the maximum soil moisture value, D_{water} is the water density (assumed to be unity) and D_{soil} is the dry porous soil density. D_{soil} is itself estimated as:

$$D_{soil} = (1 - satsm)\, D_{mine} \tag{18}$$

with $satsm$=0.4 the saturation volumetric moisture content and D_{mine}=2.5, the non-porous soil density.

This resuspension flux is calculated only for model cells having a non-zero urban landuse. This flux is thus ponderated in the whole cell by considering the relative surface of the urban area. Finally, the flux is projected onto the model size distribution considering that 2/3 of the flux is in the fine mode, 1/3 in the coarse mode. The fine and coarse modes are those defined for the anthropogenic emissions fluxes for particulate matter.

5 Processes and chemistry

5.1 Integration of the SAPRC chemical scheme

5.1.1 The general gas-phase mechanism

Two gas-phase chemical schemes were implemented in the CHIMERE model. The most detailed chemical scheme, called MELCHIOR1, represents the oxidation of around 80 gaseous species according to 300 reactions. The other mechanism, called MELCHIOR2, is a reduced version of MELCHIOR1 developed using chemical operators (Derognat et al., 2003; Carter, 1990). MELCHIOR2 represents the oxidation of around 40 gaseous species according to 120 reactions. These chemical mechanisms are described in detail in Menut et al. (2013a). Comparisons between MELCHIOR2 and ~~tree~~ three detailed mechanisms (MCM, Jenkin et al. (2003) ; SAPRC99, Carter (2000) ; GECKO-A, Aumont et al. (2005)) show a good agreement between the chemical schemes, with differences in HCHO yields under low and high NO conditions lower than 20% between the simulated results (Dufour et al., 2009). SAPRC99 chemical mechanism had already been used in CHIMERE for ~~a few~~ particular studies (Lasry et al., 2007; Coll et al., 2009) but had never been distributed in a previous CHIMERE ~~releases~~release.

Since the development of the MELCHIOR mechanisms in 2003, ~~progresses have~~ progress has been made in atmospheric chemistry, particularly concerning the VOC ozonolysis. One of the most up to date chemical ~~scheme~~ schemes currently available in the literature is the SAPRC-07 (Carter, 2010a). This mechanism is widely used and evaluated against chamber data (≈2400 experiments). The detailed SAPRC-07 chemical mechanism contains 207 species and 466 reactions. This detailed mechanism has been used to develop several reduced mechanisms designed for CTM applications (Carter, 2010b). The less reduced mechanism, SAPRC-07A, has been implemented in the 2016 CHIMERE model. This chemical scheme contains 72 species and 218 reactions. Two CHIMERE simulations using SAPRC-07A and MELCHIOR2 chemical schemes respectively were compared with AirBase measurements of NO_x and ozone over Europe during summer 2005. The two chemical schemes were found to provide ~~a~~ good correlation with ozone measurements (Pearson's correlation rate 0.71 for both mechanisms), with a slightly smaller bias for ozone concentrations obtained using SAPRC-07A (8.19 ppb versus 9.29 ppb, Menut et al. (2013a)).

5.1.2 The chlorine mechanism

Over the past decade, several studies have shown that halogens (chlorine, bromine, iodine) chemistry could influence ozone concentrations in the troposphere. A recent review by Simpson et al. (2015) presents the state of art on this topic. ~~If the~~

The role of halogen chemistry was traditionally considered limited to the marine boundary layer, recent observations have shown ~~that significant $ClNO_2$ concentrations (from 80 ppt~~ significant $ClNO_2$ concentrations from few ppt in Mid-Continental Urban Environment (Mielke et al., 2011) to 2000 ppt ~~) can occur in various environments~~in the Coastal Marine Boundary Layer (Riedel et al., 2011). This compound can act as a nitrogen reservoir with a long lifetime ~~allowing its~~ capable of long-range transport. In previous version of CHIMERE model, it was possible to have the chemical composition (Na, Cl, H_2SO_4) of sea salt emissions based on mean composition described in Seinfeld and Pandis (1997). The chlorine chemistry is not described in MELCHIOR chemical schemes but Carter (2010b) proposed in SAPRC-07A a chlorine mecha-

nism with 9 inorganic species and 3 products formed by the reactions with VOCs. In SAPRC-07A, the chlorine chemistry is represented by 68 reactions, which have been implemented in ~~CHIMERE-2016~~ CHIMERE-2017 only if the SAPRC-07A ~~chemichal~~ mechanism is chosen by the user.

5.2 Evolution of the aerosol scheme

5.2.1 ~~Disretization~~ Discretization of the aerosols size distribution

The CHIMERE model accounts for the size distribution of the aerosols using a size-bin approach: the aerosol particles for each of the model species are distributed in N size bins, covering a diameter range from D_{min} to D_{max}. Given these three user-defined parameters, a preprocessor ~~compute~~ computes a sequence $(d_i)_{i=1,N+1}$ of cutoff diameters that meets the following requirements:

- $2.5\,\mu$m and $10\,\mu$m are retained as cutoff diameters: two indices $i1$ and $i2$ such that $d_{i1} = 2.5\,\mu$m and $d_{i2} = 10\,\mu$m must exist
- The sequence of the cutoff diameters covers exactly the size interval requested by the user: $d_1 = D_{min}$ and $d_{N+1} = D_{max}$

The first requirement is set to allow a meaningful evaluation of $PM_{2.5}$ and PM_{10} in the model, since these quantities are typically available from routine measurements.

The default (and recommended) values of the extreme diameters are $D_{min} = 0.01\,\mu$m and $D_{max} = 40\,\mu$m. Using these values, the produced size distributions for various values of the number of intervals N are shown in Tab. 2 according to the requested number of bins, N. If $N \geq 12$, then the ratio of two successive cut-off diameters is always such as $d_{i+1}/d_i \leq 2$: all particles within a single size bin have comparable diameters at least within a factor 2, which is a good way to ensure that all the size-depending processes affecting the aerosols (sedimentation, coalescence etc.) are treated in a realistic way. However, when calculation speed is a critical requirement, for example for operational prevision, the number of size bins could be lowered to $N = 6$, still ensuring that $d_{i+1}/d_i \leq 4$

5.2.2 Wet diameter and ~~wet~~ density of aerosols

In many processes, the diameter and the density of aerosols are used (deposition, absorption, coagulation, etc...). These processes have to take into account that the diameter and the density of aerosols change with humidity due to the amount of water absorbed into the particles. Therefore, the notion of wet diameter and wet density was introduced in ~~CHIMERE-2016~~CHIMERE-2017. Particles are distributed between bins according to their dry diameter. The wet diameter of the particles is calculated as a function of humidity and the composition of the particle.

To compute the wet density and wet diameter for each aerosol size bin, the amount of water in each bins is computed with the ~~"reverse mode"~~ "reverse mode" of ISORROPIA (Nenes et al. (1998)) by using the composition of particles, assuming that only sulphate, nitrate, ammonium and sea salts have a high enough hygroscopicity to absorb a significant amount of water. The density of the aqueous phase of particles is computed according to composition following the method of Semmler et al. (2006). The density and mass of the inorganic aqueous phase (sulphate, nitrate, ammonium and sea salts and water) and the density and mass of other compounds (dust, organics, black carbon, etc...) are used to compute the total density of the particle and then its wet diameter, assuming internal mixing for each size bin.

5.2.3 Absorption

Absorption is described by the ~~"bulk equilibrium" approach of~~ "bulk equilibrium" approach of Pandis et al. (1993). In this approach, all the bins for which condensation is very fast are merged into a ~~"~~"bulk particulate phase~~". Following~~ ". Following Debry et al. (2007), a cutting diameter of $1.25\,\mu$m is used to separate bins which are inside the "bulk particle" (with a diameter lower than the cutting diameter) from other bins.

Thermodynamic models are used to compute the partitioning between the gas phase and the bulk particle phase and estimate the gas-phase concentrations at equilibrium. For semi-volatile inorganic species (sulphate, nitrate, ammonium), concentrations G_{eq} at equilibrium are calculated using ~~the thermodynamic module ISORROPIA()~~ISORROPIA. This model also determines the water content of particles. Equilibrium concentrations for the semivolatile organic species are related to particle concentrations through a temperature dependent partition coefficient K^p (in $m^3\mu g^{-1}$) (Pankow (1994)).

Following Pandis et al. (1993), the mass of compounds condensing into particles, ΔA_p, is redistributed over bins according to the kinetic of condensation into each bin. For evaporation, the mass of compounds evaporating from each bin is proportional to the amount of the compounds in the bin.

If the variation of particulate bulk concentration of compound i, $\Delta A_{p,i}$, is greater than 0 (condensation):

$$\Delta A_{p,i}^{bin} = \frac{k^{bin}}{\sum_j k_i^j} \Delta A_{p,i} \tag{19}$$

with k_i^{bin} the kinetic of condensation given by Seinfeld and Pandis (1997):

$$k_i^{bin} = N^{bin} \frac{2\pi D_p^{bin} D_i M_i}{RT} f(Kn, \alpha) \tag{20}$$

with N^{bin} the number of particles inside the bin, D_p^{bin} the mean diameter of the bin, D_i the diffusion coefficient for

	Number of aerosol bins													
I_v	N= 3	N= 4	N= 5	N= 6	N= 7	N= 8	N= 9	N= 10	N= 11	N= 12	N= 13	N= 14	N= 15	N= 16
1	0.01	0.01	0.01	0.01	0.01	0.01	0.01	0.01	0.01	0.01	0.01	0.01	0.01	0.01
2	2.50	0.16	0.06	0.04	0.03	0.03	0.03	0.02	0.02	0.02	0.02	0.02	0.02	0.02
3	10.00	2.50	0.40	0.16	0.09	0.09	0.06	0.05	0.05	0.04	0.03	0.03	0.03	0.03
4	40.00	10.00	2.50	0.63	0.27	0.27	0.16	0.11	0.11	0.08	0.06	0.06	0.05	0.05
5	/	40.00	10.00	2.50	0.83	0.83	0.40	0.23	0.23	0.16	0.12	0.12	0.09	0.07
6	/	/	40.00	10.00	2.50	2.50	1.00	0.52	0.52	0.32	0.21	0.21	0.16	0.12
7	/	/	/	40.00	10.00	5.00	2.50	1.14	1.14	0.63	0.40	0.40	0.27	0.20
8	/	/	/	/	40.00	10.00	5.00	2.50	2.50	1.25	0.73	0.73	0.48	0.34
9	/	/	/	/	/	40.00	10.00	5.00	5.00	2.50	1.35	1.35	0.83	0.55
10	/	/	/	/	/	/	40.00	10.00	10.00	5.00	2.50	2.50	1.44	0.92
11	/	/	/	/	/	/	/	40.00	20.00	10.00	5.00	3.97	2.50	1.51
12	/	/	/	/	/	/	/	/	40.00	20.00	10.00	6.30	3.97	2.50
13	/	/	/	/	/	/	/	/	/	40.00	20.00	10.00	6.30	3.97
14	/	/	/	/	/	/	/	/	/	/	40.00	20.00	10.00	6.30
15	/	/	/	/	/	/	/	/	/	/	/	40.00	20.00	10.00
16	/	/	/	/	/	/	/	/	/	/	/	/	40.00	20.00
17	/	/	/	/	/	/	/	/	/	/	/	/	/	40.00

Table 2. *Values of the diameter ~~bins~~ intervals, I_v (μm), obtained for $D_{min} = 0.01\,\mu$m, $D_{max} = 40\,\mu$m, and ~~twelve~~ fourteen different values of bins (N=3 to N=16).*

species i in air, M_i its molecular weight and $f(Kn, \alpha)$ is the correction due to noncontinuum effects and imperfect surface accomodation. $f(Kn, \alpha)$ is computed with the transition regime formula of Fuchs and Sutugin (1971).

If the variation of particulate bulk concentration of compound i, $\Delta A_{p,i}$, is ~~lower than 0~~ negative (evaporation):

$$\Delta A_{p,i}^{bin} = \frac{A_{p,i}^{bin}}{\sum_j A_{p,i}^{j}} \Delta A_{p,i} \tag{21}$$

If a particle shrinks or grows due to condensation/evaporation, the mass of this particle has to be redistributed over diameter bins. The mass redistribution algorithm of Gelbard and Seinfeld (1980); Seigneur (1982) is used.

5.2.4 Coagulation

The flux of coagulation $J_{coag,i}^{b}$ of a coumpound i inside a bin b is computed with the size binning method of Jacobson et al. (1994):

$$J_{coag,i}^{b} = \sum_{j=1}^{b}\sum_{k=1}^{b} f_{j,k}^{b} K_{j,l} A_{p,i}^{j} N^{k} - A_{p,i}^{b} \sum K_{b,j} N^{k} \tag{22}$$

with N^k the volumic number of particles in bin k, $K_{j,l}$ the coagulation kernel coefficient between bins i and j and $f_{j,k}^{b}$ the partition coefficient (the fraction of the particle created from the coagulation of bins j and k which is redistributed into bin b). The coagulation kernel and the partition coefficients are calculated as described in Debry et al. (2007).

5.2.5 Wet deposition

For the in-cloud scavenging of particles, the deposition of particles is assumed to be proportional to amount of water lost by precipitations. The deposition flux is written as:

$$\left[\frac{dQ_l^k}{dt}\right] = -\frac{\varepsilon_l P_r}{w_l h} Q_l^k \tag{23}$$

with P_r the precipitation rate released in the grid cell (kg m^{-2} s^{-1}), w$_l$ the liquid water content (kg m^{-3}), h the cell thickness (m) and ε_l an empirical uptake coefficient (in the range 0 - 1) currently assumed to be 1. l and k are respectively the bin and composition subscripts.

For the below-cloud scavenging of particles, particles are scavenged by raining drops following Henzig et al. (2006). A polydisperse distribution of raining drops is applied:

$$N(R) = 1.98\,10^{-5}\,\mathrm{A}\,P^{-0.384}\,R^{2.93}\exp\left(-5.38P^{-0.186}R\right) \tag{24}$$

where

$$\mathrm{A} = 1.047 - 0.0436\ln P + 0.00734\,(\ln P)^2 \tag{25}$$

with P the precipitation rate in mm/h and R the radius of the droplet. The below-cloud scavenging rate is written:

$$\left[\frac{dQ_l^k}{dt}\right] = -Q_l^k \int_R \pi R^2 u_g(R) E(R, r_l) N(R) \mathrm{d}R \tag{26}$$

with R, the radius of the raindrop (in m), r_l the radius of the particle (in m), u_g the terminal drop velocity (in m/s), $E(R, r_l)$ the collision efficiency of a particle with a raindrop, $N(R)$ (in m^{-4}) the raindrop size distribution.

5.3 Online calculation of photolysis rates using the Fast-JX module

5.3.1 Modelling strategy

~~CHIMERE-2016~~ CHIMERE-2017 includes the module Fast-JX version 7.0b (Wild et al., 2000; Bian and Prather, 2002) for the online calculation of the photolysis rates. Fast-JX is a module which solves the equations of radiative transfer in an atmospheric column taking into account the Solar ~~zenithal~~ zenith angle, the vertical profile of ozone and water vapor concentrations, the ice- and water- clouds, the radiative effect of scattering and absorption by aerosols and the surface albedo.

Following the recommendations of the Fast-JX developers, the effective size of ice particles is estimated following Heymsfield (2003) as $\mathrm{Reff}_i = 164 \times IWC^{0.23}$, where Reff_i (μm) is the effective radius of ice particles, and IWC is the ice content of the atmospheric particles (g.m^{-3}). Regarding water droplets, their radius is estimated also following the recommendations of fast-JX developers, as 9.60 μm for clouds at low altitudes (below 810 hPa), 12.68 μm for high clouds (above 610 hPa), and linearly interpolated between these two values for intermediate altitudes.

Taking these factors (and their real-time simulated variations) into account, Fast-JX computes the photolysis rates for all the relevant photochemical reactions that has been designed in order to be easily introduced in Chemistry-transport models, which has already been done in various CTMs such as PHOTOMCAT (Voulgarakis et al., 2009), Polair3D (Real and Sartelet, 2011), UKCA (Telford et al., 2013) and GEOS-Chem (Eastham et al., 2014).

CHIMERE-2013 did not take into account all of these processes (Menut et al., 2013a), relying instead on a very simplified calculation of the photolysis rates, as shown in Table 3. The photolysis rates were evaluated from tabulated values using TUV (Madronich, 1987), depending only on the solar ~~zenithal~~ zenith angle and the altitude. These tabulated values were calculated assuming a vertical profile for ozone that was typical of the northern hemisphere midlatitudes, neglecting the effect of the aerosols, and assuming a constant and uniform surface albedo. The effect of clouds was parameterized as an exponential reduction of the photolysis rates as a function of the cloud optical depth. While this set of approximations was acceptable when the CHIMERE model was used as boundary-layer regional CTM for locations in Europe, this had strong limitations for its use for longer-term simulations including long-range transport in the free troposphere over geographical domains including polar and/or tropical zones. ~~Therefore, the Fast-JX module has been included in CHIMERE-2016.~~ Photolysis rates for the photodissociation of ozone and nitrogen dioxide as computed by the Fast-JX model inside CHIMERE have been compared favorably to in situ measurements at the island of Lampedusa (Italy), including in presence of aerosols (Mailler et al., 2016)

5.3.2 surface albedo

The surface albedo in the near-UV spectral region, which is determinant for the calculation of photolysis rates Dickerson et al. (1982), is highly variable according to the landuse and to the presence or absence of snow. It is worth noting at that point that the albedo of all the continental and oceanic surfaces is smaller than 0.1, while the albedo of snow ranges from 0.3 to over 0.8 according to the type of landuse. Therefore, the absence/presence of snow will modulate very substantially the values of the modelled photolysis rates, and therefore the concentration of trace gases such as ozone. Even though strong ozone peaks generally occur in summertime in a context of strong anthropogenic NO_x production and in the absence of snow, it has been shown recently that strong ozone peaks can occur in wintertime over the continental United States in zones of oil and gas extraction due to the combination of the strong anthropogenic concentrations of VOCs in a very shallow boundary layer with relatively strong photolysis rates due to the high surface albedo (Edwards et al., 2014; Schnell et al., 2009). It is therefore important that CTMs take into account the impact of snow on surface albedo, in order to be able to reproduce correctly such cases.

The surface albedo in the UV band in ~~CHIMERE-2016~~ CHIMERE-2017 is evaluated according to Laepple et al. (2005) in the absence of snow (tested as snow depth less than 1 cm), and from Tanskannen and Manninen (2007) in the presence of snow, tested as snow depth greater than 10 cm. Values are displayed in Table 4.

The snow depth is read from the WRF or ECMWF meteorological inputs, if available. If any other model is used, the snow cover will be assumed inexistent. If the snow-cover is thinner than 1 cm in the model, the albedo is assumed to be that of dry land. If the snow-cover is thicker than 10 cm, the albedo is assumed to be that of snow-covered land. In-between, a linear interpolation is performed. Even though the case of sea-ice is not explicitly treated in Tanskannen and Manninen (2007), the assumption is made in ~~CHIMERE-2016~~ CHIMERE-2017 that the albedo of sea-ice is the same as that of a thick layer of snow covering barren land.

5.3.3 Implementation

The physical calculations performed by Fast-JX are split in two steps.

First, the Legendre coefficients for the scattering phase function for all aerosol species and diameter bin are calculated using Michael Mischenko's spher.f code (Mischenko et al., 2002), assuming sphericity of the aerosol particles.

	CHIMERE-2013	~~CHIMERE-2016~~ CHIMERE-2017
SZA	✓	✓
Altitude	✓	✓
Clouds	parameterized	✓
Tropospheric ozone column	Constant profile	✓
Stratospheric ozone column	Constant profile	Month- and latitude-dependant climatology
Water-vapor concentration	Constant profile	✓
Aerosol effect	✗	✓
Variable albedo	✗	✓

Table 3. *Taking into account the various factors affecting the photolysis rates in CHIMERE-2013 and ~~CHIMERE-2016~~CHIMERE-2017*

#	Landuse	albedo for snow	
		$<$ 1cm	$>$ 10 cm
1	Agricultural land / crops	0.035	0.376
2	GrasslandLanduse type	0.04	0.720
3	Barren land/bare ground	0.10	0.836
4	Inland Water	0.07	-
5	Urban	0.035	0.3
6	Shrubs	0.05	0.558
7	Needleaf forest	0.025	0.278
8	Broadleaf forest	0.025	0.558
9	Ocean	0.07	0.836

Table 4. *Tabulated values from Laepple et al. (2005) and Tanskannen and Manninen (2007) used for the calculation of the albedo in the UV band. In the presence of sea-ice over ocean, the albedo of the ice surface is assumed equal to the Tanskannen and Manninen (2007) value for $>$ 10 cm of snow on barren land.*

This calculation is performed for each of the $n_{spec} \times n_{bins}$ species, and for the five wavelengths that are used for the Mie scattering processes in Fast-JX. This step is performed once and for all before the first simulation step, and lasts from a couple of seconds to a couple of minutes according to the number of aerosol species and diameter bins. The refractive indices reproduced in Table 5 are the ones provided along with the model, essentially based on ~~results from the ADIENT project~~the values compiled in the framework of the ADIENT project[2], as described by the corresponding technical report by E. J. Highwood[3]. However, the specification of these parameters is in a parameter file, and can be changed by the user to other values. In the same way, the user can easily introduce more species in the optical treatment for specific studies, e.g. volcanic ashes.

After the preprocessing phase, at each time step and in each model column, the Fast-JX module resolves the radiative transfer in the model atmospheric column, computing the actinic fluxes at each model level and integrating them over N wavelength bins in order to produce accurate photolysis rates. In the configuration adopted for ~~CHIMERE-2016~~CHIMERE-2017, N is set to 12, which is the value ~~recommanded~~ recommended by Fast-JX developers for tropospheric studies. These 12 wavelength bins include the 7 standard Fast-J wavelength bins from 291 nm to 850 nm, as described in Wild et al. (2000). The 7 standard Fast-J wavelength bins are essentially concentrated from 291 nm to 412.5 nm which is the spectral band relevant for tropospheric photochemistry. Following the ~~recommandations~~ recommendations of Fast-JX model developers, these 7 standard wavelength bins are complemented by 5 additional wavelength bins, from 202.5 nm to 291 nm, which are only relevant in the upper tropical troposphere. In a typical simulation framework, it has been found that the increase in computational time relative to the simulation with tabulated photolysis rates is below 10% (Mailler et al., 2016).

5.4 Online calculation of lidar profiles

During the model integration, some additional diagnostic variables are estimated: (i) the Clouds Optical depth (COD) and the Aerosol Optical Depth (AOD) using the FastJX module, and (ii) the lidar profiles.

The lidar profiles are calculated using the ~~aerosols concentrations~~ aerosol contributions only, as detailed in Stromatas et al. (2012). They are proposed as output after a simulation and are designed to be directly comparable to ground-based or spatial lidars. Three different profiles are calculated both in Nadir and Zenith lidar configurations: (i) the Attenuated Scattering Ratio, $R'(z)$, (ii) $\beta'(z,\lambda)$ and $\beta'_{\mathrm{m}}(z,\lambda)$, respectively the total and molecular attenuated backscatter signal.

By definition, $R'(z)$ is equal to 1 in absence of aerosols/clouds and when the signal is not attenuated. In the presence of aerosols, $R'(z)$ would be greater than one. Following Winker et al. (2009), this ratio is expressed as:

$$R'(z) = \frac{\beta'(z)}{\beta'_{\mathrm{m}}(z)} \quad (27)$$

[2] http://www.reading.ac.uk/adient/refractiveindices.html, visited Jan. 17, 2017

[3] www.reading.ac.uk/adient/REFINDS/Techreportjul09.doc, visited Jan. 17, 2017

Species	Real part of the refractive index					Imaginary part of the refractive index				
λ	200 nm	300 nm	400 nm	600 nm	1000 nm	200 nm	300 nm	400 nm	600 nm	1000 nm
PPM	1.53	1.52	1.52	1.51	1.50	$8.0{\cdot}10^{-3}$	$8.0{\cdot}10^{-3}$	$8.0{\cdot}10^{-3}$	$8.0{\cdot}10^{-3}$	$8.0{\cdot}10^{-3}$
OCAR	1.60	1.60	1.63	1.63	1.63	$1.2{\cdot}10^{-1}$	$1.2{\cdot}10^{-1}$	$7.7{\cdot}10^{-2}$	$1.2{\cdot}10^{-2}$	$7.0{\cdot}10^{-2}$
BCAR	1.85	1.85	1.85	1.85	1.85	$7.1{\cdot}10^{-1}$	$7.1{\cdot}10^{-1}$	$7.1{\cdot}10^{-1}$	$7.1{\cdot}10^{-1}$	$7.1{\cdot}10^{-1}$
SALT	1.38	1.38	1.37	1.36	1.35	$8.7{\cdot}10^{-7}$	$3.5{\cdot}10^{-7}$	$6.6{\cdot}10^{-9}$	$1.2{\cdot}10^{-8}$	$2.6{\cdot}10^{-5}$
SOA	1.56	1.56	1.56	1.56	1.56	$3.0{\cdot}10^{-3}$	$3.0{\cdot}10^{-3}$	$3.0{\cdot}10^{-3}$	$3.0{\cdot}10^{-3}$	$3.0{\cdot}10^{-3}$
DUST	1.53	1.53	1.53	1.53	1.53	$5.5{\cdot}10^{-3}$	$5.5{\cdot}10^{-3}$	$2.4{\cdot}10^{-3}$	$8.9{\cdot}10^{-4}$	$7.6{\cdot}10^{-4}$
H2SO4	1.50	1.47	1.44	1.43	1.42	$1.0{\cdot}10^{-8}$	$1.0{\cdot}10^{-8}$	$1.0{\cdot}10^{-8}$	$1.3{\cdot}10^{-8}$	$1.2{\cdot}10^{-6}$
HNO3	1.53	1.53	1.53	1.53	1.53	$6.0{\cdot}10^{-3}$	$6.0{\cdot}10^{-3}$	$6.0{\cdot}10^{-3}$	$6.0{\cdot}10^{-3}$	$6.0{\cdot}10^{-3}$
NH3	1.53	1.52	1.52	1.52	1.52	$5.0{\cdot}10^{-4}$	$5.0{\cdot}10^{-4}$	$5.0{\cdot}10^{-4}$	$5.0{\cdot}10^{-4}$	$5.0{\cdot}10^{-4}$
WATER	1.35	1.34	1.34	1.33	1.33	$2.0{\cdot}10^{-9}$	$2.0{\cdot}10^{-9}$	$1.8{\cdot}10^{-8}$	$3.4{\cdot}10^{-8}$	$3.9{\cdot}10^{-7}$

Table 5. *Refractive indices for the main aerosol species in CHIMERE at 200, 300, 400, 600 and 1000 nm*

The total attenuated backscatter signal $\beta'(z,\lambda)$ is calculated as:

$$\beta'(z,\lambda) = \left[\frac{\sigma_{\rm m}^{\rm sca}(z,\lambda)}{S_{\rm m}(z,\lambda)} + \frac{\sigma_{\rm p}^{\rm sca}(z,\lambda)}{S_{\rm p}(z,\lambda)}\right] \exp\left(-2\left[\int_z^{\rm TOA} \sigma_{\rm m}^{\rm ext}(z',\lambda){\rm d}z' + \eta' \int_z^{\rm TOA} \sigma_{\rm p}^{\rm ext}(z',\lambda){\rm d}z'\right]\right) \quad (28)$$

and the molecular attenuated backscatter signal $\beta'_{\rm m}(z,\lambda)$ as:

$$\beta'_{\rm m}(z,\lambda) = \frac{\sigma_{\rm m}^{\rm sca}(z,\lambda)}{S_{\rm m}(z,\lambda)} \cdot \exp\left(-2\int_{\rm z}^{\rm TOA} \sigma_{\rm m}^{\rm ext}({\rm z}',\lambda){\rm d}z'\right) \quad (29)$$

$\sigma_{\rm p}^{\rm sca/ext}(z,\lambda)$ and $\sigma_{\rm m}^{\rm sca/ext}(z,\lambda)$ are the extinction/scattering coefficients for particles and molecules (in $\rm km^{-1}$). $S_{\rm m}$ and $S_{\rm p}$ are the molecular and particular extinction-to-backscatter ratios (in sr). $\eta'(z)$ represents the particles multiple scattering and z represents the distance between the emitter and the studied point. Note that for the case of a space lidar the integration begins from the top of the atmosphere (TOA) while for a ground lidar the integration begins from 0 (ground level) to z. Further details about these calculations are provided in Stromatas et al. (2012).

6 Model scores for ~~a standard European simulation~~two test cases over Europe

The performance of CTMs is often evaluated by comparing simulation results to data of measurements, either from routine networks (Solazzo et al., 2012a, b) or from dedicated field campaigns (e.g. ~~).~~ Menut et al. (2015); Petetin et al. (2015)). Simon et al. (2012) presented an overview of performance evaluation studies for a large set of models and studied cases.

Species	Winter	Summer
O3	~~98~~ 96	93
NO2	~~39~~ 40	~~35~~ 34
SO2	~~14~~ 12	~~29~~ 27
PM10	~~28~~ 26	~~22~~ 20
PM25	~~23~~ 22	~~17~~ 16

Table 6. *Number of EMEP stations per species and per season used for performance statistics. Stations CH01 CH04 CH05 DE03 DE08 AT05 AT48 IT01 IT04 ES78 DE44 were excluded from the analysis due to their topography difficult to simulate with a 0.5° resolution.*

~~In this study statistical validation with data of measurements was~~ A statistical evaluation with measurement data is performed for two ~~3-month~~ 3-months long simulations with ~~CHIMERE-2016~~CHIMERE-2017: summer (June to August 2008) and winter (January to March 2009). Each of the simulation periods analyzed was preceeded by a 15-day spinup period. The simulation domain covers western and central Europe at 0.5° resolution, with 8 vertical sigma levels between 997 and 500 hPa. The meteorological model used was WRF 3.6.1 with the same physical options as in (Menut et al., 2015), ~~at~~ xpat 45 km resolution and boundary conditions from GFS analyses. The emission data were those from EMEP at 0.5°, and the boundary conditions for the concentrations from the LMDz-INCA model for gases and chemically active aerosols and from the GOCART model for dust. The simulation was performed with the MELCHIOR2 chemical mechanism for gaseous species, 10 bins for aerosol size distribution and the SOA scheme of Bessagnet et al. (2008), 5-min chemistry time step, and the Van Leer numerical scheme for both horizontal and vertical transport. The (Wesely, 1989) aerosol dry deposition and (Loosmore, 2003) resuspension schemes were used. The

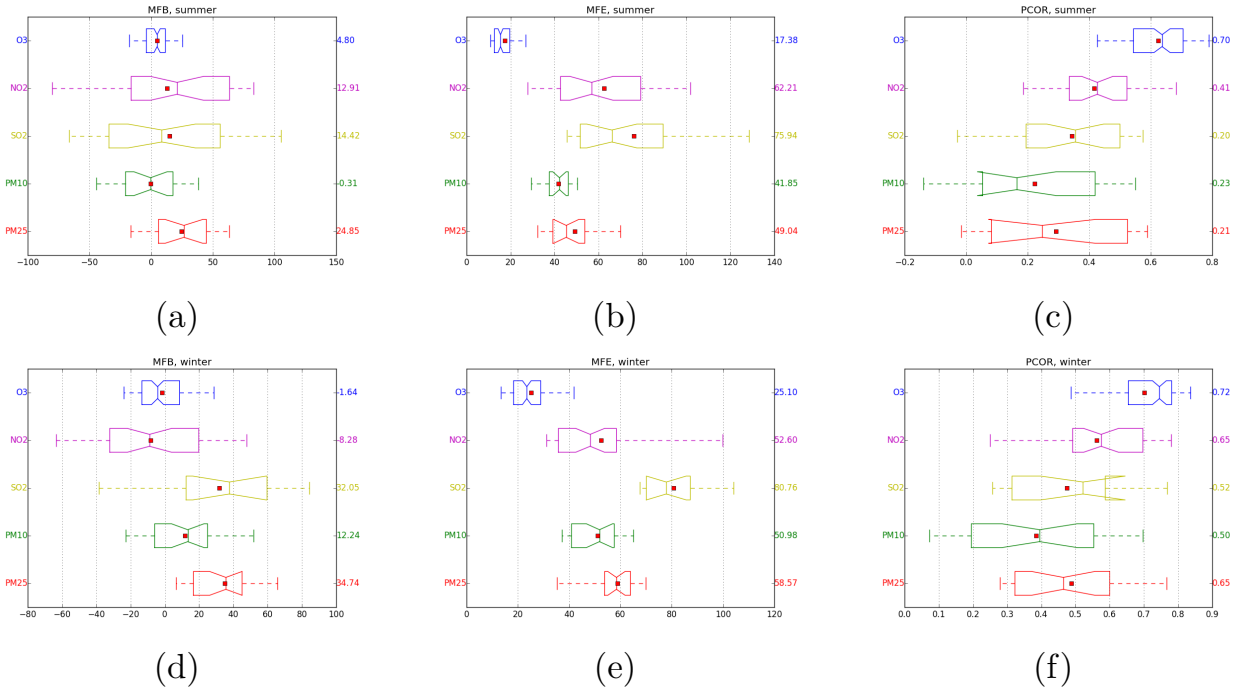

Figure 8. *Performance statistics for the main model species and for daily averaged values. The numbers on the right axes give the ~~Person~~overall scores (Pearson's correlation, MFE, and MFB), while the box plots show the variability among the EMEP stations. The boxes extend from the lower to upper quartile values of the data. The center lines show the medians, and the red squares show the means over stations. The whiskers indicate the 5 and 95 percentile values, and the values on the right axis of each panel are the overall value of the considered indicator, i.e. merging all the stations into a single statistical dataset as described in Jacobson (2005)*

online coupling with ISORROPIA model was ~~not activated, and the precalculated lookup tables were usedinstead~~ used.

The statistical scores ~~were computed against the EMEP~~ are computed between modelled and observed daily averaged values, using surface concentration measurements ~~for main gaseous and aerosol species~~from the EMEP moditoring sites, after filtering out the stations with complex topography (CH01 CH04 CH05 DE03 DE08 AT05 AT48 IT01 IT04 ES78 DE44) that cannot be simulated appropriately at 0.5° resolution. Stations from the EMEP monitoring sites have been chosen for this study because their location has been selected in order to minimize local influences and be representative of large areas (Tørseth et al., 2012). For each simulation period only stations containing at least 70% of time series data were retained.

Figure ~~??~~ 8 shows the performance statistics for the main model species. The number of EMEP stations used for each species for winter and summer is shown in Table ~~??~~6. The standard metrics used for air quality modeling (Simon et al., 2012) were employed, namely the Pearson's correlation $PCOR$, the mean fractional error MFE, and the mean fractional bias MFB.

Ozone shows the best scores among all the species, both for summer and winter, with ~~$PCOR = 0.69$, $MFE = 19.6\%$, $MFB = 11.4$~~ $PCOR = 0.70$, $MFE = 17\%$, $MFB = 5\%$ in summer and $PCOR = 0.72$, ~~$MFE = 24.9\%$, $MFB = 14.8$~~ $MFE = 25\%$, $MFB = 2\%$ in winter. It also shows the smallest variability of scores among the stations (~~96~~ 93 available stations in summer and ~~98~~ 96 in winter). As noted by Simon et al. (2012), the ozone overestimation often reported for CTMs is related to the averaging over the hours with high and low concentrations, so the scores are dominated by performance at low concentrations, which occur much more often than high concentrations. Indeed, the MFB computed from daily maximum ozone concentrations ~~in this study~~ (not shown) is quite lower: ~~1.5~~1% for summer and ~~3.6~~7% for winter.

The NO_2 shows quite larger MFE: ~~54.9 % in winter and 60.4% in summer~~ 62% in summer and 53% in winter, with a large variability of both MFE and MFB between stations. The bias is negative in winter, slightly positive in summer but with a high negative values (NO_2 underestimation) at some stations. ~~The~~ For this particular species, with strong emissions horizontal gradients, the model resolution of 0.5 ~~might be not enough to represent the large NO_x emission gradients, even when~~ ° is not enough even when surface concentrations are measured at the background rural sites. Also, as discussed

by refbterrenoire2015Terrenoire et al. (2015), the negative bias can be related to the general underestimation of the emissions in the inventory used, especially during the traffic daily peaks. This is in agreement with the relatively high correlation: 0.65 in winter and 0.41 in summer.

The SO_2 shows the largest MFE for both summer (74.576%) and winter (80.281%) and quite low the lowest correlation in summer (0.20). It shows positive biasin winter: $MFB = 35.5\%$ $MFB = 32\%$ in winter and 14% in summer. The difficulty of in SO_2 simulation can could be related to the emission profile, in particular the vertical distribution of emitted speciesuncertainties in the emission vertical profiles, which is a particularly sensitive factor in SO_2 modelling, because industrial stack emissions represent a substantial part of SO_2 emissions (Pirovano et al., 2012; Mailler et al., 2013). While some CTMs have included a plume-in-grid model for subgrid treatment of point emissions depending on the actual meteorological conditions and flux characteristics, this is not the case of the CHIMERE model, which can also limit the performance of the model regarding SO_2 concentrations. The conversion of SO_2 to sulphate can also be a source of error in SO_2 concentrations, as mentioned by Ciarelli et al. (2016) and Bessagnet et al. (2016), who observed very different behaviour of models far from emission sources, probably due to the chemical mechanisms. The lower correlation coefficient in summertime was found in all the CTMs examined in Bessagnet et al. (2016).

The performance for PM is affected by compensating effects of several chemical components, such as dust, primary organics and secondary species like sulphates, nitrates, and SOA.

The PM_{10} concentrations are generally overestimated in winter ($MFB = 15.6\%$). The particulate nitrate HNO_3 and ammonium NH_4 contribute to this overestimation. The correlation values are $MFB = 12\%$), with correlation values lower in winter (0.460.50) and summer (0.250.23) than for the whole year(and hence in autumn in spring), as reported by refbterrenoire2015Terrenoire et al. (2015). In summer the PM_{10} bias is quie low $MFB = 2.8$quite low $MFB \approx 0\%$, and the MFE (40.0 42%) shows small variability between the stations.

The PM_{25} concentrations show slightly a larger overestimation than PM_{10} in winter ($MFB = 35\%$ vs 12% for PM_{10}) and have also a positive bias in summer ($MFB = 25\%$). The winter correlation is higher though (0.60 vs 0.460.65 vs 0.50), and its variablility variability between the stations is smaller. This might indicate that the dust, whose emissions are very sensitive to the wind speed, contribute to the PM_{10} errors in winter. As suggested by refbterrenoire2015, the PMThe PM_{25} overestimation is likely to be related can be associated to the overestimation of sulphate. ammoniac ($MFB = 77\%$ in summer and 65% in winter) and sulphate ($MFB = 32\%$ in summer and 33% in winter, not shown).

The EPA guidelines, (e.g.) , define the Boylan and Russell (2006) define performance goals and criteria to be attained by air quality models. The Their performance goal is attained for particulate matter when the MFE is less or equal to 50%, and |MFB| is less than 30%. The performance criteria are attained when the MFE is less or equal to 75%, and |MFB| is less than 60%. The performance goal is thus a more demanding condition than the performance criteria.

The PM_{10} simulation satisfies the performance goal for both summer and winter. As for PM_{25}, it satisfies the performance goal in terms of MFB for both summer and winter and in terms of MFE in summer, but fails in terms of MFE in winter ($MFE = 53.4\%$). However it does satify summer and the performance criteria for both seasonsin winter.

7 Application to the Puyehue-Cordon Caulle eruption (June 2011)

A simulation with the present version of CHIMERE has been performed for the southern hemisphere, from May 15 to June 30, 2011, a period covering the eruption of Puyehue-Cordon Caulle (Chile). This eruption has emitted an important plume containing volcanic ashes and sulphur dioxide into the troposphere and the lower stratosphere. This plume has had severe consequences on air traffic over Argentina as well as other countries in the southern hemisphere. While the eruption began on June 4, the plume went all around the around the entire southern hemisphere and was back in the vicinity of the emission source by June 14 (Global Volcanism Program, 2013; Klüser et al., 2013). This volcanic eruption case provides a perfect testbed to evaluate the new abilities of the CHIMERE model to simulate as accurately as possible transport at hemispheric scale, including cases where the transported plume undergoes a complete circumpolar trajectory around the South Pole.

7.1 Model configuration

The meteorological simulation has been performed using the WRF meteorological model, version 3.5.1, on a simulation domain covering most of the southern hemisphere at a resolution of about 55 x 55 km at 45°S.

The CHIMERE model has been used in the following configuration : with 20 vertical levels from the surface to 200 hPa100 hPa. For the gasous chemistry, the MELCHIOR-2 chemical mechanism 250x250 horizontal domain has been used. The horizontal domain is composed of 250x250 cells and is centered at the south pole and covering the entire extratropical southern hemisphereHorizontal resolution . The horizontal resolution varies with latitude: 65km x 65km (at the pole), 55 x 55 km (at 45°S), 36 x 36 km at at 25°S. Including

The anthropogenic and biogenic emissions are taken into account and produced from the HTAP dataset and MEGAN model, respectively. Mineral dust emissions have not been included in this simulation, since the focus of this testbed study was in the circumpolar transport of ash emissions from the Puyehue volcano. The novely of this simulation is the addition of the volcanic emissions of SO_2 and volcanic ashes.

7.2 Volcanic emissions

The total mass flux emitted in the form of particles has been represented according to Mastin et al. (2009), using the following equation,

$$\dot{V} = \left(\frac{H}{2.00}\right)^{\frac{1}{2.41}}$$
$$\dot{M} = \rho \dot{V} \quad (30)$$

where H is the column height expressed in km, $\dot{V}$ is the volume flux expressed in $\mathrm{m^3\,s^{-1}}$, $\dot{M}$ is the mass flux in $\mathrm{kg\,s^{-1}}$ and $\rho = 2500\,\mathrm{kg\,m^{-3}}$ is the ash density. The altitude of the ash column has been taken from Collini et al. (2013), and is reproduced here in Table 7. Only the fine fraction of the emissions, with particle diameter smaller than 63 μm has been included. The conversion from the total emitted mass flux has been performed using a conversion factor m_{63} taken from Mastin et al. (2009) for S2 type volcanoes~~.~~, i.e. $m_{63} = 0.4$. It is worth noting at this point that the uncertainty on the value of this parameter, m_{63}, is very strong, with values ranging from 0.02 to 0.6 depending on the characteristics of the considered eruption, and that therefore the uncertainties on the resulting mass of fine ash is very strong. The particles emitted with a diameter greater than ~~80~~63μm have not been considered because they are not supposed to be relevant for long-range transport due to their rapid sedimentation.

The emitted ashes have been distributed evenly from the altitude of the crater (2200 m.a.s.l) to the altitude of the top of the column, obtained by summing the column height to the altitude of the crater. ~~However, for June 4, 5 and 6 the altitude of the top of the volcanic plume has been limited to 11000m.a.s.l to avoid loss of volcanoc ashes throuht the top of the model, which is located at 180 hPa, or equivalently 12000 m.a.s.l at the considered latitude.~~

The refractive indices of the volcanic ashes from Derimian et al. (2012) have been used. However, as these authors provide the refractive indices of volcanic ash only in the visible, the values at 200 and 300 nm have been taken as equal to the value given at 440 nm.

The granulometry of the ashes are taken as 80% in a coarse mode, with a lognormal distribution centered at 30 μm and 20% in a finer mode with a lognormal distribution centered at 4 μm, consistent with the results of Durant et al. (2009).

The SO_2 mass flux has been ~~adapted from~~ taken from Theys et al. (2013), who prescribe mass flux estimates based on IASI measurements for the first 48 hours of the eruption. Since these authors do not provide an estimation for the subsequent part of the eruption, we ~~completed the time series for SO_2 emission by assuming a constant ratio between the mass flux of the ash, provided by , and the~~ assumed that the SO_2 ~~mass flux (see Tab. 8).~~ fluxes are null after the 48 first hours of the eruption. This hypothesis is of course questionable, but nevertheless the study of Theys et al. (2013) shows in a convincing way that most of the SO_2 emission occurs during the first 48 hours of the eruption.

day	H	$\dot{V}$	$\dot{M}$	M	M_{63}
04/06	10	794.9	1.99×10^{06}	2.86×10^{10}	1.14×10^{10}
05/06	10	794.9	1.99×10^{06}	1.72×10^{11}	6.87×10^{10}
06/06	10	794.9	1.99×10^{06}	1.72×10^{11}	6.87×10^{10}
07/06	6.5	133.0	3.33×10^{05}	2.87×10^{10}	1.15×10^{10}
08/06	7	180.9	4.52×10^{05}	3.91×10^{10}	1.56×10^{10}
09/06	8.5	405.0	1.01×10^{06}	8.75×10^{10}	3.50×10^{10}
10/06	8	314.9	7.87×10^{05}	6.80×10^{10}	2.72×10^{10}
11/06	6.5	133.0	3.33×10^{05}	2.87×10^{10}	1.15×10^{10}
12/06	7	180.9	4.52×10^{05}	3.91×10^{10}	1.56×10^{10}
13/06	8	314.9	7.87×10^{05}	6.80×10^{10}	2.72×10^{10}
14/06	7	240.9	6.02×10^{05}	5.20×10^{10}	2.08×10^{10}
15/06	8	314.9	7.87×10^{05}	6.80×10^{10}	2.72×10^{10}
16/06	7	180.9	4.52×10^{05}	3.91×10^{10}	1.56×10^{10}
17/06	5.5	66.5	1.66×10^{05}	1.44×10^{10}	5.75×10^{09}
18/06	5	44.8	1.12×10^{05}	9.68×10^{09}	3.87×10^{09}
19/06	4	17.7	4.44×10^{04}	3.83×10^{09}	1.53×10^{09}
20/06	4	17.7	4.44×10^{04}	3.83×10^{09}	1.53×10^{09}

Table 7. *Main characteristics of the volcanic emissions used for the hemispheric simulation. H : column height (km) ; $\dot{V}$: volume flux ($m^3\,s^{-1}$); $\dot{M}$: Mass flux ($kg\,s^{-1}$); M : emitted mass (kg); M_{63} : emitted mass for the fraction with diameter $< 63\mu m$*

~~07/06 - 00-24UTC 6.5 60 2.01×10^7 08/06 - 00-24UTC 7 60 2.74×10^7 09/06 -~~

Table 8. H : column height (km) ; $\dot{M}$: Mass flux ($kt\,d^{-1}$); M : emitted mass of SO_2 (kg)

7.3 ~~Anthropogenic and natural emissions~~Analysis of the circumpolar transport

~~Anthropogenic and natural emissions have been modelled as described above. The anthropogenic emissions have been produced from the HTAP dataset, while biogenic emissions have been produced from the MEGAN model. Mineral dust emissions have not been included in this simulation, since the focus of this testbed study was in the circumpolar transport of ash emissions from the Puyehue volcano.~~

7.4 ~~Simulation outputs~~

7.3.1 ~~Circumpolar transport~~

The simulation is initialized by climatological concentrations for aerosols and trace gases from the LMDZ-INCA Chemistry-transport model. These two datasets are also used to provide the top and lateral boundary conditions during the simulation. The simulation itself, covering from May 15 through June 30 can be divided into two successive phases : first, from May 14 to June 4, the model undergoes a spinup period, with the concentrations of gaseous and particulate species building up due to the emissions of sea-salt and anthropogenic contaminants (Fig. 9a). At the end of this spin-up period, ~~significan~~ significant AOD values, from 0.05 to 0.20 appear over the southern ocean from 30 to 70°S, mostly due to sea-salt emissions, consistent with the findings of Jaeglé et al. (2011), and consistent with the satellite-based climatology of these authors, which represent a mean value about 0.15 in these areas. In the subsequent time steps, the volcanic ash plume from the Puyehue volcano becomes the dominant feature of the AOD structure in the southern hemisphere. While it is difficult to compare the simulated values to measured ones because of the large uncertainties on the mass flux and size distribution of the volcanic ashes, it is possible to compare the modelled trajectory of the ash plume with spaceborne observations. For this purpose, we will rely on the space images and analyses provided by ~~and~~ Klüser et al. (2013) and Global Volcanism Program (2013). Fig. 9b for June 6 at 12UTC (8AM local time) can be compared to Figure 2 of Klüser et al. (2013) (lower left panel), which shows that at this time, about 36 hours after the onset of the eruption, the initial direction of the volcanic plume is eastward, with a slight southward tilt, consistent with the CHIMERE simulations. On June 8 (Fig. 9d), the simulated pattern for ash transport also fits very well the pattern that is visible on Fig. 3 by these authors (upper left panel), with the initial portion of the ash plume travelling southward over the southern Atlantic and reaching towards the southern Pacific ocean over cape Horn, a pattern that is observed in both CHIMERE observations and the satellite observations. The older parts of the plume are located either off the Atlantic coasts of Argentina, covering a large part of southern Brazil in the model but not so in the infrared AOD data provided by Klüser et al. (2013). Finally, the plume from the initial explosions are located at that time in the ~~souther~~ southern ocean, in-between the southern tip of the African continent and the Antarctic. It can also be observed that while the ash plume is continuous in the CHIMERE simulation, it is not so in the observations. This reflects the succession of explosive phases and quiet phases of the volcanic eruption, while the flux imposed to the CHIMERE model is continuous, as discussed in Boichu et al. (2013), who also present a possible workaround for this problem by assimilation of satellite data.

Four days later, on June 12, the leading edge of the volcanic ash plume is located at about 135°W and 55°S above the southern Pacific ocean, while other portions of the plume are located above New-Zealand, Tasmania, and areas of continental Australia and South-Africa. Later on, on June 14, the leading edge of the ash plume reaches back to the southern coasts of Chile, as visible in both the simulation outputs (Fig. 9f) and the report of Global Volcanism Program (2013), indicating that part of the plume was reaching South-America from the Pacific ocean at that time between 35 and 50°S while other parts of the ash plume were located further to the South, close to the Antarctic peninsula, consistent with Fig. 9f. On June 14 and during the following days, the plume from the initial explosion of June 4 and the following days is overpassing the Puyehue volcano again, a fact that is correctly captured by the CHIMERE model.

7.3.1 ~~Lidar observables~~

~~As described in Section 5.4, the main LIDAR observables are now provided as model outputs by the CHIMERE model. As an example of the results of this treatment for the case of the Puyehue eruption, the zenithal and nadir simulated backscattering ratios are presented on Fig. ??. Even though a validation of these observables by confrontation to observations is not presented here, the simulated patterns are physically reasonable, with backscattering rations reaching maximum values in the lowest part of the aerosol plumes (for the zenithal backscattering ratio, Fig. ??a) and low values above due to absorption and scattering of the beam by the lowest part of the plume. Of course, the contrary is observed for the simulated space-based nadir backscatter ratio (Fig. ??b)~~

~~(a) Zenithal backscattering ratio as simulated by CHIMERE at 1000 nm wavelength above the city of Buenos Aires ; and (b), same as (a) but for the Nadir backscattering ratio~~

8 Conclusions

~~CHIMERE-2016~~ CHIMERE-2017 is a model version which presents several major improvements compared to the earlier version described in ~~. The version presented here has the ability to include all types of emissions.~~ Menut et al. (2013a). Compared to the previous model version, anthropogenic emissions can be generated anywhere in the world from the HTAP emission inventory, as well as mineral dust emissions, which were available only for North Africa and the Arabian peninsula in previous model versions. With the same objective of permitting the use of the model in any part of the world and at any scale from urban to hemispheric scale, an important limitation of the model has been removed by improving the internal treatment of the transport on the sphere, allowing for domains up to the hemispheric scale, and pos-

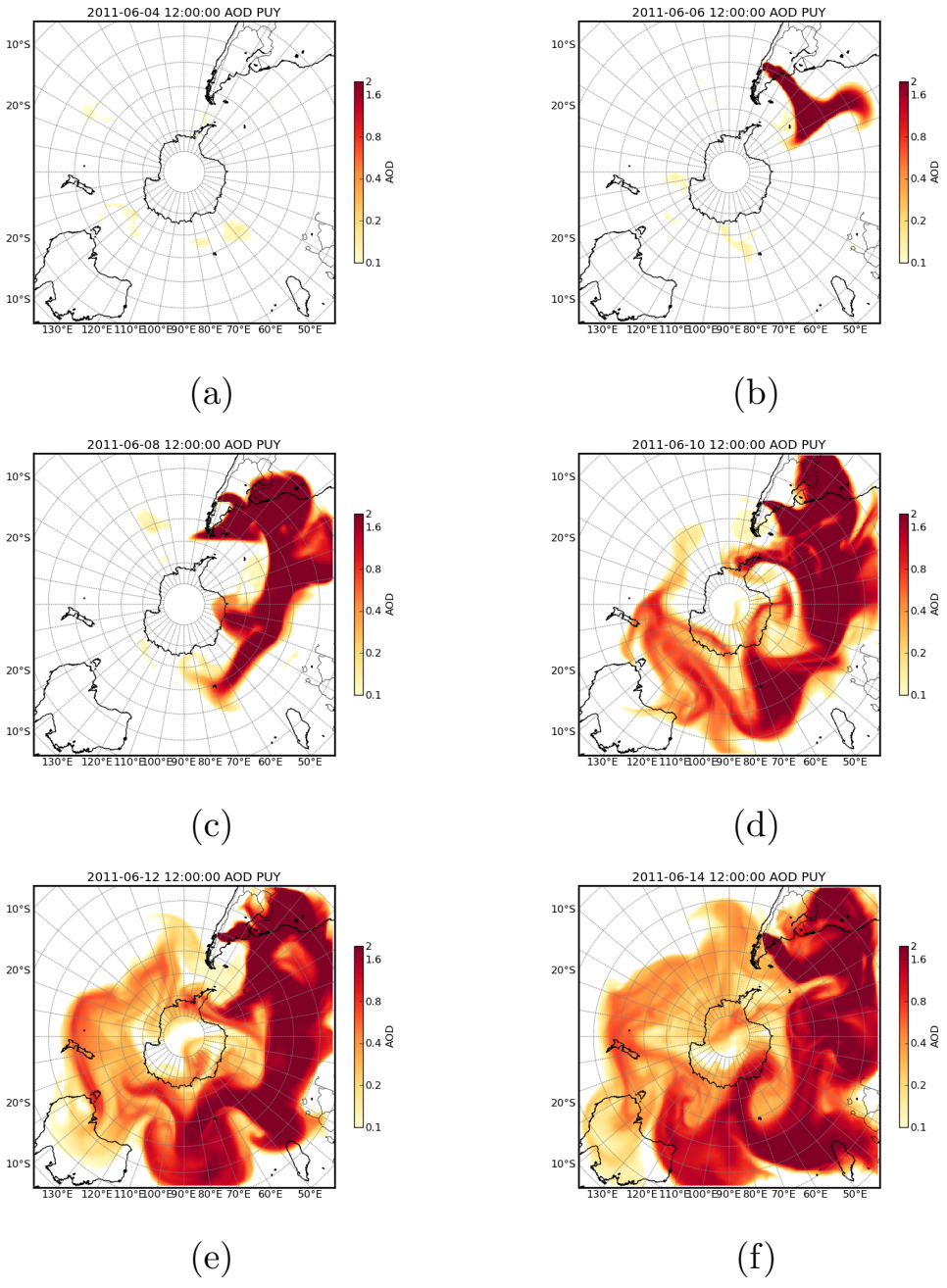

Figure 9. *Simulated AOD at 600 nm every 48 hours from June 4, 12UTC to June 14, ~~12UTC~~12:00 UTC*

sibly including a geographic pole. Much attention has also been paid to the physical processes, including a major update in the representation of the physical processes affecting the aerosols, as well as the effect of the modelled aerosol on the photolytic reaction rates. Other efforts have been made to improve the user's experience with the model: this includes improvements in the parallelization of the model in order to reduce computation time, as well as providing key observable variables such as the Aerosol optical depth and LIDAR backscatter coefficients, which permits the user to compare the outputs of the model directly with the results of remote-sensing observations.

These improvements pave the way to many applications that were out of reach for the CHIMERE model up to now: CHIMERE 2016 has the necessary abilities to give new insights on questions such as the radiative impact of aerosols

on photochemistry, at all scales, from urban to hemispheric, including mineral dust emissions and deposition anywhere in the world. The possibility to run hemispheric simulations also allows the use of this CTM for the study of transport of aerosol and gaseous contamination plumes between the different continent within a hemisphere. It contributes to bridge the gap between global chemistry-transport models such as LMDz-INCA, MOZART or Geos-CHEM and regional models: while CHIMERE has already been used successfully for the evaluation of the decadal trends in air quality over Europe (Colette et al., 2011), as shown by the study Xing et al. (2015) with the hemispheric version of CMAQ, hemispheric versions of regional CTMs are tools that can be used successfully to study long-term trends in regional air quality with added value from models simulated in regional domains only because they can perform a consistent simulation over the entire hemisphere without relying on boundary conditions provided by global CTMs relying on different assumptions and parameterizations.

Code availability

The present article refers to the ~~CHIMERE-2016~~ CHIMERE-2017 release, which is freely available and provided under the GNU general public licence[4]. The source code along with the corresponding technical documentation can be obtained from the CHIMERE web site at http://www.lmd.polytechnique.fr/chimere/.

Acknowledgements. For anthropogenic emissions, EuroglobalMap products includes Intellectual Property from European National Mapping and Cadastral Authorities and is licensed on behalf of these by EuroGeographics. Original product is freely available at www.eurogeographics.org. Terms of the licence available at http://www.eurogeographics.org/form/topographic-data-eurogeographics.

The MACC boundary conditions data set was provided by the MACC-II project, which is funded through the European Union Framework 7 programme. It is based on the MACC-II reanalysis for atmospheric composition; full access to and more information about this data can be obtained through the MACC-II web site http://www.copernicus-atmosphere.eu. We acknowledge C.Prigent for providing the global high resolution aeolian aerodynamic roughness length.

References

Alfaro, S. C. and Gomes, L.: Modeling mineral aerosol production by wind erosion: Emission intensities and aerosol size distributions in source areas, Journal of Geophysical Research: Atmospheres, 106, 18 075–18 084, doi:10.1029/2000JD900339, 2001.

Arakawa, A. and Lamb, V. R.: Computational Design of the Basic Dynamical Processes of the {UCLA} General Circulation Model, in: General Circulation Models of the Atmosphere, edited by Chang, J., vol. 17 of *Methods in Computational Physics: Advances in Research and Applications*, pp. 173 – 265, Elsevier, doi:10.1016/B978-0-12-460817-7.50009-4, 1977.

Aumont, B., Szopa, S., and Madronich, S.: Modelling the evolution of organic carbon during its gas-phase tropospheric oxidation: development of an explicit model based on a self generating approach, Atmos Chem Phys, pp. 2497–2517, 2005.

Beegum, S., I.Gherboudj, N.Chaouch, F.Couvidat, L.Menut, and H.Ghedira: Simulating Aerosols over Arabian Peninsula with CHIMERE: Sensitivity to soil, surface parameters and anthropogenic emission inventories, Atmospheric Environment, 128, 185–197, doi:10.1016/j.atmosenv.2016.01.010, 2016.

Bessagnet, B., Menut, L., Aymoz, G., Chepfer, H., and Vautard, R.: Modelling dust emissions and transport within Europe: the Ukraine March 2007 event, Journal of Geophysical Research, 113, D15 202, doi:10.1029/2007JD009541, 2008.

Bessagnet, B., Pirovano, G., Mircea, M., Cuvelier, C., Aulinger, A., Calori, G., Ciarelli, G., Manders, A., Stern, R., Tsyro, S., García Vivanco, M., Thunis, P., Pay, M.-T., Colette, A., Couvidat, F., Meleux, F., Rouïl, L., Ung, A., Aksoyoglu, S., Baldasano, J. M., Bieser, J., Briganti, G., Cappelletti, A., D'Isidoro, M., Finardi, S., Kranenburg, R., Silibello, C., Carnevale, C., Aas, W., Dupont, J.-C., Fagerli, H., Gonzalez, L., Menut, L., Prévôt, A. S. H., Roberts, P., and White, L.: Presentation of the EURODELTA III intercomparison exercise – evaluation of the chemistry transport models' performance on criteria pollutants and joint analysis with meteorology, Atmospheric Chemistry and Physics, 16, 12 667–12 701, doi:10.5194/acp-16-12667-2016, http://www.atmos-chem-phys.net/16/12667/2016/, 2016.

Bian, H. and Prather, M.: Fast-J2: accurate simulation of stratospheric photolysis in global chemical models, J. Atmos. Chem., 41, 281–296, 2002.

Bieser, J., Aulinger, A., Matthias, V., Quante, M., and Denier van der Gon, H.: Vertical emission profiles for Europe based on plume rise calculations., Environ. Pollut., 159, 2935–2946, doi:10.1016/j.envpol.2011.04.030, 2011.

Boichu, M., Menut, L., Khvorostyanov, D., Clarisse, L., Clerbaux, C., Turquety, S., and Coheur, P.-F.: Inverting for volcanic SO2 flux at high temporal resolution using spaceborne plume imagery and chemistry-transport modelling: the 2010 Eyjafjallajokull eruption case-study, Atmos Chem Phys, 13, 8569–8584, doi:10.5194/acp-13-8569-2013, 2013.

Boylan, J. W. and Russell, A. G.: PM and light extinction model performance metrics, goals, and criteria for three-dimensional air quality models, Atmos. Env., 40, 4946–4959, 2006.

Carter, W.: Development of the SAPRC-07 chemical mechanism, Atmos Environ, 44, 5324 – 5335, doi:10.1016/j.atmosenv.2010.01.026, 2010a.

Carter, W.: Development of a condensed SAPRC-07 chemical mechanism, Atmos Environ, 44, 5336 – 5345, 2010b.

Carter, W. P. L.: A detail mechanism for the gas-phase atmospheric reactions of organic compounds, Atmos Environ, 24, 481–518, 1990.

Carter, W. P. L.: Documentation of the SAPRC-99 chemical mechanism for VOC reactivity assessment: Final report to California Air Resources Board, Contract 92-329 and Contract 95-308, California Air Resources Board, Sacramento, Calif., 2000.

[4]http://www.gnu.org/copyleft/gpl.html

Ciarelli, G., Aksoyoglu, S., Crippa, M., Jimenez, J.-L., Nemitz, E., Sellegri, K., Äijälä, M., Carbone, S., Mohr, C., O'Dowd, C., Poulain, L., Baltensperger, U., and Prévôt, A. S. H.: Evaluation of European air quality modelled by CAMx including the volatility basis set scheme, Atmospheric Chemistry and Physics, 16, 10 313–10 332, doi:10.5194/acp-16-10313-2016, http://www.atmos-chem-phys.net/16/10313/2016/, 2016.

Colella, P. and Woodward, P. R.: The piecewise parabolic method (PPM) for gas-dynamical simulations, Journal of Computational Physics, 11, 38–39, 1984.

Colette, A., Granier, C., Hodnebrog, Ø., Jakobs, H., Maurizi, A., Nyiri, A., Bessagnet, B., D'Angiola, A., D'Isidoro, M., Gauss, M., Meleux, F., Memmesheimer, M., Mieville, A., Rouïl, L., Russo, F., Solberg, S., Stordal, F., and Tampieri, F.: Air quality trends in Europe over the past decade: a first multi-model assessment, Atmospheric Chemistry and Physics, 11, 11 657–11 678, doi:10.5194/acp-11-11657-2011, http://www.atmos-chem-phys.net/11/11657/2011/, 2011.

Coll, I., Lasry, F., Fayet, S., Armengaud, A., and Vautard, R.: Simulation and evaluation of 2010 emission control scenarios in a Mediterranean area, Atmos Environ, 43, 4194 – 4204, 2009.

Collini, E., Osores, M. S., Folch, A., Viramonte, J. G., Villarosa, G., and Salmuni, G.: Volcanic ash forecast during the June 2011 Cordón Caulle eruption, Natural Hazards, 66, 389–412, doi:10.1007/s11069-012-0492-y, 2013.

Copernicus: Atmosphere Monitoring Services, http://macc-raq.copernicus-atmosphere.eu/, accessed: 2017-03-13, 2017.

Debry, E., Fahey, K., Sartelet, K., Sportisse, B., and Tombette, M.: Technical Note: A new SIze REsolved Aerosol Model (SIREAM), Atmos. Chem. Phys., 7, 1537–1547, doi:10.5194/acp-7-1537-2007, http://www.atmos-chem-phys.net/7/1537/2007/, 2007.

Derimian, Y., Dubovik, O., Tanre, D., Goloub, P., Lapyonok, T., and Mortier, A.: Optical properties and radiative forcing of the Eyjafjallajokull volcanic ash layer observed over Lille, France, in 2010, Journal of Geophysical Research: Atmospheres, 117, n/a–n/a, doi:10.1029/2011JD016815, 2012.

Derognat, C., Beekmann, M., Baeumle, M., Martin, D., and Schmidt, H.: Effect of biogenic volatile organic compound emissions on tropospheric chemistry during the Atmospheric Pollution Over the Paris Area (ESQUIF) campaign in the Ile-de-France region, Journal of Geophysical Research, 108, doi:10.1029/2001JD001421, 2003.

Dickerson, R. R., Stedman, D. H., and Delany, A. C.: Direct measurements of ozone and nitrogen dioxide photolysis rates in the troposphere, Journal of Geophysical Research: Oceans, 87, 4933–4946, doi:10.1029/JC087iC07p04933, http://dx.doi.org/10.1029/JC087iC07p04933, 1982.

Dufour, G., Wittrock, F., Camredon, M., Beekmann, M., Richter, A., and Aumont, B.: SCIAMACHY formaldehyde observations: constraint for isoprene emission estimates over Europe?, Atmos Chem Phys, 9, 1647–1664, 2009.

Durant, A. J., Rose, W. I., Sarna-Wojcicki, A. M., Carey, S., and Volentik, A. C. M.: Hydrometeor-enhanced tephra sedimentation: Constraints from the 18 May 1980 eruption of Mount St. Helens, Journal of Geophysical Research: Solid Earth, 114, n/a–n/a, doi:10.1029/2008JB005756, 2009.

Eastham, S. D., Weisenstein, D. K., and Barrett, S. R.: Development and evaluation of the unified tropospheric–stratospheric chemistry extension (UCX) for the global chemistry-transport model GEOS-Chem, Atmospheric Environment, 89, 52 – 63, doi:http://dx.doi.org/10.1016/j.atmosenv.2014.02.001, http://www.sciencedirect.com/science/article/pii/S1352231014000971, 2014.

Edwards, P. M., Brown, S. S., Roberts, J. M., Ahmadov, R., Banta, R. M., deGouw, J. A., Dubé, W. P., Field, R. A., Flynn, J. H., Gilman, J. B., Graus, M., Helmig, D., Koss, A., Langford, A. O., Lefer, B. L., Lerner, B. M., Li, R., Li, S.-M., McKeen, S. A., Murphy, S. M., Parrish, D. D., Senff, C. J., Soltis, J., Stutz, J., Sweeney, C., Thompson, C. R., Trainer, M. K., Tsai, C., Veres, P. R., Washenfelder, R. A., Warneke, C., Wild, R. J., Young, C. J., Yuan, B., and Zamora, R.: High winter ozone pollution from carbonyl photolysis in an oil and gas basin, Nature, 514, 351–354, doi:10.1038/nature13767, 2014.

Fecan, F., Marticorena, B., and Bergametti, G.: Parameterization of the increase of aeolian erosion threshold wind friction velocity due to soil moisture for arid and semi-arid areas, Annals of Geophysics, 17, 149–157, 1999.

Friedrich, R. and Reis, S.: Emissions of Air Pollutants – Measurements, Calculation, Uncertainties – Results from the EUROTRAC-2 Subproject GENEMIS, Springer Publishers, Berlin, Heidelberg, Germany, 2004.

Fuchs, N. and Sutugin, A.: Topics in current aerosol research (part 2), chap. High dispersed aerosols, Pergamon, New york, 1971.

Gallego, F. J.: A population density grid of the European Union, Population and Environment, 31, 460–473, doi:10.1007/s11111-010-0108-y, http://dx.doi.org/10.1007/s11111-010-0108-y, 2010.

Gelbard, F. and Seinfeld, J. H.: Simulation of multicomponent aerosol dynamics, Journal of colloid and Interface Science, 78, 485–501, 1980.

Global Volcanism Program: Report on Puyehue-Cordon Caulle (Chile), in: Bulletin of the Global Volcanism Network, 38:9, edited by Wunderman, R., Smithsonian Institution, doi:10.5479/si.GVP.BGVN201309-357150, 2013.

Grini, A., Myhre, G., Zender, C. S., and Isaksen, I.: Model simulations of dust sources and transport in the global atmosphere: Effects of soil erodibility and wind speed variability, J. Geophys. Res., 110, D02 205, doi:10.1029/2004JD005037, 2005.

Halpern, B. S., Frazier, M., Potapenko, J., Casey, K. S., Koenig, K., Longo, C., Stewart Lowndes, J., Rockwood, R. C., Selig, E. R., Selkoe, K. A., and Walbridge, S.: Spatial and temporal changes in cumulative human impacts on the world's ocean, Nature Communications, 6, doi:10.1038/ncomms8615, 2015.

Henzig, J. S., Olivié, D., and van Velthoven, P.: A parameterization of size resolved below cloud scavenging of aerosols by rain, Atmos. Chem. Phys., 6, 3363–3375, 2006.

Heymsfield, A.: Properties of Tropical and Midlatitude Ice Cloud Particle Ensembles. Part I: Median Mass Diameters and Terminal Velocities, Journal of the Atmospheric Sciences, 60, 2573–2591, doi:10.1175/1520-0469(2003)060<2573:POTAMI>2.0.CO;2, 2003.

Homer, C., Huang, C., Yang, L., Wylie, B., and Coan, M.: Development of a 2001 National Landcover Database for the United States., Photogrammetric Engineering and Remote Sensing, 70, 829–840, 2004.

Honoré, C., Rouïl, L., Vautard, R., Beekmann, M., Bessagnet, B., Dufour, A., Elichegaray, C., Flaud, J., Malherbe, L., Meleux,

F., Menut, L., Martin, D., Peuch, A., Peuch, V., and Poisson, N.: Predictability of European air quality: The assessment of three years of operational forecasts and analyses by the PREV'AIR system, Journal of Geophysical Research, 113, D04 301, doi:10.1029/2007JD008761, 2008.

Inness, A., Baier, F., Benedetti, A., Bouarar, I., Chabrillat, S., Clark, H., Clerbaux, C., Coheur, P., Engelen, R. J., Errera, Q., Flemming, J., George, M., Granier, C., Hadji-Lazaro, J., Huijnen, V., Hurtmans, D., Jones, L., Kaiser, J. W., Kapsomenakis, J., Lefever, K., Leitão, J., Razinger, M., Richter, A., Schultz, M. G., Simmons, A. J., Suttie, M., Stein, O., Thépaut, J.-N., Thouret, V., Vrekoussis, M., Zerefos, C., and the MACC team: The MACC reanalysis: an 8 yr data set of atmospheric composition, Atmospheric Chemistry and Physics, 13, 4073–4109, doi:10.5194/acp-13-4073-2013, http://www.atmos-chem-phys.net/13/4073/2013/, 2013.

Ishizuka, M., Mikami, M., Leys, J., Yamada, Y., Heidenreich, S., Shao, Y., and McTainsh, G. H.: Effects of soil moisture and dried raindroplet crust on saltation and dust emission, Journal of Geophysical Research: Atmospheres, 113, n/a–n/a, doi:10.1029/2008JD009955, http://dx.doi.org/10.1029/2008JD009955, d24212, 2008.

Iversen, J. D. and White, B. R.: Saltation threshold on Earth, Mars and Venus, Sedimentology, 29, 111–119, 1982.

Jacobson, M., Turco, R., Jensen, E., and Toon, O.: Modeling coagulation among particles of different composition and size, Atmos. Environ., 28, 1327–1338, 1994.

Jacobson, M. Z.: Fundamentals of atmospheric modelling (sencond edition), p. 697, Cambridge University Press, 2005.

Jaeglé, L., Quinn, P. K., Bates, T. S., Alexander, B., and Lin, J.-T.: Global distribution of sea salt aerosols: new constraints from in situ and remote sensing observations, Atmospheric Chemistry and Physics, 11, 3137–3157, doi:10.5194/acp-11-3137-2011, http://www.atmos-chem-phys.net/11/3137/2011/, 2011.

Jenkin, M. E., Saunders, S. M., Wagner, V., and Pilling, M. J.: Protocol for the development of the Master Chemical Mechanism, MCM v3 (Part B): tropospheric degradation of aromatic volatile organic compounds, Atmos Chem Phys, 3, 181–193, 2003.

Klüser, L., Erbertseder, T., and Meyer-Arnek, J.: Observation of volcanic ash from Puyehue - Cordón Caulle with IASI, Atmos. Meas. Tech., 6, 36–46, doi:10.5194/amt-6-35-2013, 2013.

Kok, J. F., Albani, S., Mahowald, N. M., and Ward, D. S.: An improved dust emission model Ž2013 Part 2: Evaluation in the Community Earth System Model, with implications for the use of dust source functions, Atmospheric Chemistry and Physics, 14, 13 043–13 061, doi:10.5194/acp-14-13043-2014, http://www.atmos-chem-phys.net/14/13043/2014/, 2014a.

Kok, J. F., Mahowald, N. M., Fratini, G., Gillies, J. A., Ishizuka, M., Leys, J. F., Mikami, M., Park, M.-S., Park, S.-U., Van Pelt, R. S., and Zobeck, T. M.: An improved dust emission model Ž2013 Part 1: Model description and comparison against measurements, Atmospheric Chemistry and Physics, 14, 13 023–13 041, doi:10.5194/acp-14-13023-2014, http://www.atmos-chem-phys.net/14/13023/2014/, 2014b.

Laepple, T., Schultz, M. G., Lamarque, J. F., Madronich, S., Shetter, R. E., Lefer, B. L., and Atlas, E.: Improved albedo formulation for chemistry transport models based on satellite observations and assimilated snow data and its impact on tropospheric photochemistry, Journal of Geophysical Research: Atmospheres, 110, doi:10.1029/2004JD005463, 2005.

Lasry, F., Coll, I., Fayet, S., Havre, M., and Vautard, R.: Short-term measures for the control of ozone peaks: expertise from CTM simulations, Journal of Atmospheric Chemistry, 57, 107–134, 2007.

Lattuati, M.: Contribution à l'étude du bilan de l'ozone troposphérique à l'interface de l'Europe et de l'Atlantique Nord: modélisation lagrangienne et mesures en altitude, Thèse de sciences, Université Paris 6, France, 1997.

Li, J., keng Liao, W., Choudhary, A., Ross, R., Thakur, R., Gropp, W., Latham, R., Siegel, A., Gallagher, B., and Zingale, M.: Parallel netCDF: A High-Performance Scientific I/O Interface, SC Conference, 0, 39, doi:http://doi.ieeecomputersociety.org/10.1109/SC.2003.10053, 2003.

Loosmore, G. A.: Evaluation and development of models for resuspension of aerosols at short times after deposition, Atmospheric Environment, 37, 639 – 647, doi:http://dx.doi.org/10.1016/S1352-2310(02)00902-0, 2003.

Madronich, S.: Photodissociation in the atmosphere: 1. Actinic flux and the effects of ground reflections and clouds, Journal of Geophysical Research: Atmospheres, 92, 9740–9752, doi:10.1029/JD092iD08p09740, http://dx.doi.org/10.1029/JD092iD08p09740, 1987.

Mahowald, N., Albani, S., Kok, J. F., Engelstaeder, S., Scanza, R., Ward, D. S., and Flanner, M. G.: The size distribution of desert dust aerosols and its impact on the Earth system, Aeolian Research, 15, 53 – 71, doi:http://dx.doi.org/10.1016/j.aeolia.2013.09.002, http://www.sciencedirect.com/science/article/pii/S1875963713000736, 2014.

Mailler, S., Khvorostyanov, D., and Menut, L.: Impact of the vertical emission profiles on ground-level gas-phase pollution simulated from the EMEP emissions over Europe, Atmos. Chem. Phys., 13, 5987–5998, doi:doi:10.5194/acp-13-5987-2013, 2013.

Mailler, S., Menut, L., di Sarra, A. G., Becagli, S., Di Iorio, T., Bessagnet, B., Briant, R., Formenti, P., Doussin, J.-F., Gómez-Amo, J. L., Mallet, M., Rea, G., Siour, G., Sferlazzo, D. M., Traversi, R., Udisti, R., and Turquety, S.: On the radiative impact of aerosols on photolysis rates: comparison of simulations and observations in the Lampedusa island during the ChArMEx/ADRIMED campaign, Atmospheric Chemistry and Physics, 16, 1219–1244, doi:10.5194/acp-16-1219-2016, http://www.atmos-chem-phys.net/16/1219/2016/, 2016.

Markakis, K., Valari, M., Perrussel, O., Sanchez, O., and Honore, C.: Climate-forced air-quality modeling at the urban scale: sensitivity to model resolution, emissions and meteorology, Atmospheric Chemistry and Physics, 15, 7703–7723, doi:10.5194/acp-15-7703-2015, http://www.atmos-chem-phys.net/15/7703/2015/, 2015.

Marticorena, B. and Bergametti, G.: Modelling the atmospheric dust cycle: 1-Design a soil-derived dust emissions scheme, Journal of Geophysical Research, 100, 16 415–16 430, 1995.

Mastin, L., Guffanti, M., Servranckx, R., Webley, P., Barsotti, S., Dean, K., Durant, A., Ewert, J., Neri, A., Rose, W., Schneider, D., Siebert, L., Stunder, B., Swanson, G., Tupper, A., Volentik, A., and Waythomas, C.: A multidisciplinary effort to assign realistic source parameters to models of volcanic

ash-cloud transport and dispersion during eruptions, Journal of Volcanology and Geothermal Research, 186, 10 – 21, doi:http://dx.doi.org/10.1016/j.jvolgeores.2009.01.008, http://www.sciencedirect.com/science/article/pii/S0377027309000146, improved Prediction and Tracking of Volcanic Ash Clouds, 2009.

Menut, L., Vautard, R., Beekmann, M., and Honoré, C.: Sensitivity of Photochemical Pollution using the Adjoint of a Simplified Chemistry-Transport Model, J. Geophys. Res., 105, 15 379–15 402, 2000.

Menut, L., Bessagnet, B., Khvorostyanov, D., Beekmann, M., Blond, N., Colette, A., Coll, I., Curci, G., Foret, F., Hodzic, A., Mailler, S., Meleux, F., Monge, J., Pison, I., Siour, G., Turquety, S., Valari, M., Vautard, R., and Vivanco, M.: CHIMERE 2013: a model for regional atmospheric composition modelling, Geoscientific Model Development, 6, 981–1028, doi:10.5194/gmd-6-981-2013, 2013a.

Menut, L., Perez Garcia-Pando, C., Haustein, K., Bessagnet, B., Prigent, C., and Alfaro, S.: Relative impact of roughness and soil texture on mineral dust emission fluxes modeling, Journal of Geophysical Research, 118, 6505–6520, doi:10.1002/jgrd.50313, 2013b.

Menut, L., Mailler, S., Siour, G., Bessagnet, B., Turquety, S., Rea, G., Briant, R., Mallet, M., Sciare, J., Formenti, P., and Meleux, F.: Ozone and aerosol tropospheric concentrations variability analyzed using the ADRIMED measurements and the WRF and CHIMERE models, Atmospheric Chemistry and Physics, 15, 6159–6182, doi:10.5194/acp-15-6159-2015, http://www.atmos-chem-phys.net/15/6159/2015/, 2015.

Menut, L., Goussebaile, A., Bessagnet, B., Khvorostiyanov, D., and Ung, A.: Impact of realistic hourly emissions profiles on air pollutants concentrations modelled with CHIMERE, ATMOSPHERIC ENVIRONMENT, 49, 233–244, doi:10.1016/j.atmosenv.2011.11.057, 2012.

Middleton, P., Stockwell, W. R., and Carter, W. P.: Agregation and analysis of volatile organic compound emissions for regional modelling, Atmospheric Environemnt, 24, 1107–1133, 1990.

Mielke, L. H., Furgeson, A., and Osthoff, H. D.: Observation of CINO2 in a Mid-Continental Urban Environment, Environ. Sci. Tech., 45, 8889–8896, iSI Document Delivery No.: 831BU, 2011.

Mischenko, M., Travis, L. D., and Lacis, A. A.: Scattering, absorption and emission of light by small particles, Cambridge University Press, Cambridge, 2002.

Monks, P., Granier, C., Fuzzi, S., Stohl, A., Williams, M., Akimoto, H., Amann, M., Baklanov, A., Baltensperger, U., Bey, I., Blake, N., Blake, R., Carslaw, K., Cooper, O., Dentener, F., Fowler, D., Fragkou, E., Frost, G., Generoso, S., Ginoux, P., Grewe, V., Guenther, A., Hansson, H., Henne, S., Hjorth, J., Hofzumahaus, A., Huntrieser, H., Isaksen, I., Jenkin, M., Kaiser, J., Kanakidou, M., Klimont, Z., Kulmala, M., Laj, P., Lawrence, M., Lee, J., Liousse, C., Maione, M., McFiggans, G., Metzger, A., Mieville, A., Moussiopoulos, N., Orlando, J., O'Dowd, C., Palmer, P., Parrish, D., Petzold, A., Platt, U., Pöschl, U., Prévôt, A., Reeves, C., Reimann, S., Rudich, Y., Sellegri, K., Steinbrecher, R., Simpson, D., ten Brink, H., Theloke, J., van der Werf, G., Vautard, R., Vestreng, V., Vlachokostas, C., and von Glasow, R.: Atmospheric composition change - global and regional air quality, Atmospheric Environment, 43, 5268 – 5350, doi:http://dx.doi.org/10.1016/j.atmosenv.2009.08.021, 2009.

Nenes, A., Pilinis, C., and Pandis, S.: ISORROPIA: A new thermodynamic model for inorganic multicomponent atmospheric aerosols, Aquatic Geochem., 4, 123–152, 1998.

Pandis, S. N., Wexler, A., and Seinfeld, J. H.: Secondary organic aerosol formation and transport. II. Predicting the ambient secondary aerosol size distribution, Atmospheric Environemnt, 27, 2403–2416, 1993.

Pankow, J. F.: An absorption model of gas/aerosol partition involved in the formation of secondary organic aerosol, Atmospheric Environemnt, 28, 189–193, 1994.

Passant, N.: Speciation of UK emissions of non-methane volatile organic compounds, Tech. Rep. ENV-0545, AEA technology, Culham (UK), http://uk-air.defra.gov.uk/assets/documents/reports/empire/AEAT_ENV_0545_final_v2.pdf, 2002.

Petetin, H., Beekmann, M., Colomb, A., Denier van der Gon, H. A. C., Dupont, J.-C., Honoré, C., Michoud, V., Morille, Y., Perrussel, O., Schwarzenboeck, A., Sciare, J., Wiedensohler, A., and Zhang, Q. J.: Evaluating BC and NO_x emission inventories for the Paris region from MEGAPOLI aircraft measurements, Atmospheric Chemistry and Physics, 15, 9799–9818, doi:10.5194/acp-15-9799-2015, http://www.atmos-chem-phys.net/15/9799/2015/, 2015.

Pirovano, G., Balzarini, A., Bessagnet, B., Emery, C., Kallos, G., Meleux, F., Mitsakou, C., Nopmongcol, U., Riva, G., and Yarwood, G.: Investigating impacts of chemistry and transport model formulation on model performance at European scale, Atmospheric Environment, 53, 93 – 109, doi:10.1016/j.atmosenv.2011.12.052, 2012.

Prigent, C., Jiménez, C., and Catherinot, J.: Comparison of satellite microwave backscattering (ASCAT) and visible/near-infrared reflectances (PARASOL) for the estimation of aeolian aerodynamic roughness length in arid and semi-arid regions, Atmos. Meas. Tech., 5, 2703–2712, 2012.

Rao, S., Galmarini, S., and Puckett, K.: Air Quality Model Evaluation International Initiative (AQMEII): Advancing the State of the Science in Regional Photochemical Modeling and Its Applications, Bull. Amer. Meteor. Soc., 92, 23–30, 2011.

Real, E. and Sartelet, K.: Modeling of photolysis rates over Europe: impact on chemical gaseous species and aerosols, Atmos. Chem. Phys, 11, 1711–1727, doi:10.5194/acp-11-1711-2011, 2011.

Riedel, T. P., Bertram, T. H., Crisp, T. A., Williams, E. J., Lerner, B. M., Vlasenko, A., Li, S. M., Gilman, J., de Gouw, J., Bon, D. M., Wagner, N. L., Brown, S. S., and Thornton, J. A.: Nitryl Chloride and Molecular Chlorine in the Coastal Marine Boundary Layer, Environ. Sci. Tech., 46, 10 463–10 470, 2011.

Schaap, M., Vautard, R., Bergstrom, R., van Loon, M., Bessagnet, B., Brandt, J., Christensen, H., Cuvelier, K., Foltescu, V., Graff, A., E., J. J., Kerschbaumer, A., Krol, M., Langner, J., Roberts, P., Rouil, L., Stern, R., Tarrason, L., Thunis, P., Vignati, E., White, L., Wind, P., and Builtjes, P. H. J.: Evaluation of long-term aerosol simulations from seven air quality models and their ensemble in the EURODELTA study, Atmospheric Environemnt, 41, 2083–2097, 2007.

Schnell, R. C., Oltmans, S. J., Neely, R. R., Endres, M. S., Molenar, J. V., and White, A. B.: Rapid photochemical production of ozone at high concentrations in a rural site during winter, Nature Geosciences, 2, 120–122, doi:10.1038/ngeo415, 2009.

Seigneur, C.: A model of sulfate aerosol dynamics in atmospheric plumes, Atmos. Environ., 16, 2207–2228, 1982.

Seinfeld, J. H. and Pandis, S. N.: Atmospheric chemistry and physics: From air pollution to climate change, Wiley-Interscience, 1997.

Semmler, M., Luo, B. P., and Koop, T.: Densities of liquid H+/NH4+/SO42-/NO3-/H2O solutions at tropospheric temperatures, Atmos. Environ., 40, 467–483, 2006.

Shao, Y. and Lu, I.: A simple expression for wind erosion threshold friction velocity, J. Geophys. Res., 105, 22,437–22,443, 2000.

Simon, H., Baker, K., and Phillips, S.: Compilation and interpretation of photochemical model performance statistics published between 2006 and 2012, Atmospheric Environment, 61, 124–139, doi:10.1016/j.atmosenv.2012.07.012, 2012.

Simpson, D., Benedictow, A., Berge, H., Bergström, R., Emberson, L. D., Fagerli, H., Flechard, C. R., Hayman, G. D., Gauss, M., Jonson, J. E., Jenkin, M. E., Nyíri, A., Richter, C., Semeena, V. S., Tsyro, S., Tuovinen, J.-P., Valdebenito, A., and Wind, P.: The EMEP MSC-W chemical transport model - technical description, Atmospheric Chemistry and Physics, 12, 7825–7865, doi:10.5194/acp-12-7825-2012, http://www.atmos-chem-phys.net/12/7825/2012/, 2012.

Simpson, W. R., Brown, S. S., Saiz-Lopez, A., Thornton, J. A., and von Glasow, R.: Tropospheric Halogen Chemistry: Sources, Cycling, and Impacts, CHEMICAL REVIEWS, 115, 4035–4062, 2015.

Solazzo, E., Bianconi, R., Pirovano, G., Matthias, V., Vautard, R., Moran, M. D., Appel, K. W., Bessagnet, B., Brandt, J., Christensen, J. H., Chemel, C., Coll, I., Ferreira, J., Forkel, R., Francis, X. V., Grell, G., Grossi, P., Hansen, A. B., Miranda, A. I., Nopmongcol, U., Prank, M., Sartelet, K. N., Schaap, M., Silver, J. D., Sokhi, R. S., Vira, J., Werhahn, J., Wolke, R., Yarwood, G., Zhang, J., Rao, S. T., and Galmarini, S.: Operational model evaluation for particulate matter in Europe and North America in the context of AQMEII, Atmospheric Environment, 53, 75 – 92, doi:10.1016/j.atmosenv.2012.02.045, http://www.sciencedirect.com/science/article/pii/S1352231012001604, 2012a.

Solazzo, E., Bianconi, R., Vautard, R., Appel, K. W., Moran, M. D., Hogrefe, C., Bessagnet, B., Brandt, J., Christensen, J. H., Chemel, C., Coll, I., van der Gon, H. D., Ferreira, J., Forkel, R., Francis, X. V., Grell, G., Grossi, P., Hansen, A. B., Jericevic, A., Kraljevic, L., Miranda, A. I., Nopmongcol, U., Pirovano, G., Prank, M., Riccio, A., Sartelet, K. N., Schaap, M., Silver, J. D., Sokhi, R. S., Vira, J., Werhahn, J., Wolke, R., Yarwood, G., Zhang, J., Rao, S., and Galmarini, S.: Model evaluation and ensemble modelling of surface-level ozone in Europe and North America in the context of AQMEII, Atmospheric Environment, 53, 60–74, doi:10.1016/j.atmosenv.2012.01.003, 2012b.

Stromatas, S., Turquety, S., Menut, L., Chepfer, H., Cesana, G., Pere, J., and Bessagnet, B.: Lidar signal simulation for the evaluation of aerosols in chemistry-transport models, Geoscientific Model Development, 5, 2012.

Tanskannen, A. and Manninen, T.: Effective UV surface albedo of seasonally snow-covered lands, Atmos. Chem. Phys., 7, 2759–2764, 2007.

Telford, P. J., Abraham, N. L., Archibald, A. T., Braesicke, P., Dalvi, M., Morgenstern, O., OĆonnor, F. M., Richards, N. A. D., and Pyle, J. A.: Implementation of the Fast-JX photolysis scheme (v6.4) into the UKCA component of the MetUM chemistry-climate model (v7.3), Geosci. Model Dev., 6, 161–177, doi:10.5194/gmd-6-161-2013, 2013.

Terrenoire, E., Bessagnet, B., Rouïl, L., Tognet, F., Pirovano, G., Létinois, L., Beauchamp, M., Colette, A., Thunis, P., Amann, M., and Menut, L.: High-resolution air quality simulation over Europe with the chemistry transport model CHIMERE, Geoscientific Model Development, 8, 21–42, doi:10.5194/gmd-8-21-2015, http://www.geosci-model-dev.net/8/21/2015/, 2015.

Theys, N., Campion, R., Clarisse, L., Brenot, H., van Gent, J., Dils, B., Corradini, S., Merucci, L., Coheur, P.-F., Van Roozendael, M., Hurtmans, D., Clerbaux, C., Tait, S., and Ferrucci, F.: Volcanic SO_2 fluxes derived from satellite data : a survey using OMI, GOME-2, IASI and MODIS, Atmos. Chem. Phys., 13, 5945–5968, doi:10.5194/acp-13-5945-2013, 2013.

Tiedtke, M.: A comprehensive mass flux scheme for cumulus parameterization in large-scale models, Mon Weather Rev, 117, 1779–1800, 1989.

Tørseth, K., Aas, W., Breivik, K., Fjæraa, A. M., Fiebig, M., Hjellbrekke, A. G., Lund Myhre, C., Solberg, S., and Yttri, K. E.: Introduction to the European Monitoring and Evaluation Programme (EMEP) and observed atmospheric composition change during 1972-2009, Atmospheric Chemistry and Physics, 12, 5447–5481, doi:10.5194/acp-12-5447-2012, http://www.atmos-chem-phys.net/12/5447/2012/, 2012.

Valari, M. and Menut, L.: Does increase in air quality models resolution bring surface ozone concentrations closer to reality?, Journal of Atmospheric and Oceanic Technology, doi:10.1175/2008JTECHA1123.1, 2008.

Valari, M. and Menut, L.: Transferring the heterogeneity of surface emissions to variability in pollutant concentrations over urban areas through a chemistry transport model, Atmos Environ, 44, 3229–3238, 2010.

Van Leer, B.: Towards the ultimate conservative difference scheme. V A second order sequel to Godunov's method, J. Computational Phys., 32, 101–136, 1979.

Vautard, R., B.Bessagnet, M.Chin, and Menut, L.: On the contribution of natural Aeolian sources to particulate matter concentrations in Europe: testing hypotheses with a modelling approach, Atmospheric Environment, 39, 3291–3303, 2005.

Vautard, R., Builtjes, P. H. J., Thunis, P., Cuvelier, K., Bedogni, M., Bessagnet, B., Honoré, C., Moussiopoulos, N., G., P., Schaap, M., Stern, R., Tarrason, L., and Van Loon, M.: Evaluation and intercomparison of Ozone and PM10 simulations by several chemistry-transport models over 4 European cities within the City-Delta project, Atmospheric Environemnt, 41, 173–188, 2007.

Vidic, S.: Frequency distribution of Effective Plume Height, Internal technical note, EMEP, Oslo, Norway, 2002.

Voulgarakis, A., Savage, N. H., Wild, O., Carver, G. D., Clemitshaw, K. C., and Pyle, J. A.: Upgrading photolysis in the PHOTOMCAT CTM: model evaluation and assessment of the role of clouds, Geosci. Model Dev., 2, 59–72, doi:10.5194/gmd-2-59-2009, 2009.

Vuolo, M. R., Menut, L., and Chepfer, H.: Impact of transport schemes on modeled dust concentrations, J. Atmos. Oceanic Technol., 26, 1135–1143, 2009.

Wesely, M.: Parameterization of Surface Resistances to Gaseous Dry Deposition in Regional-Scale Numerical Models, Atmospheric Environemnt, 23, 1293–1304, 1989.

Wild, O., Zhu, X., and Prather, J.: Fast-J: accurate simulation of the in- and below-cloud photolysis in tropospheric chemical models, J. Atmos. Chem., 37, 245–282, 2000.

Winker, D. M., M. A. Vaughan, A. O., Hu, Y., Powell, K. A., Liu, Z., Hunt, W. H., and Young, S. A.: Overview of the CALIPSO Mission and CALIOP Data Processing Algorithms, Journal of Atmospheric and Oceanic Technology, 26, 2009.

Wolock, D.: State soil geographic (STATSGO) data base-data use information, Tech. rep., US Department of Agriculture, 1994.

Xing, J., Mathur, R., Pleim, J., Hogrefe, C., Gan, C.-M., Wong, D. C., Wei, C., Gilliam, R., and Pouliot, G.: Observations and modeling of air quality trends over 1990–2010 across the Northern Hemisphere: China, the United States and Europe, Atmospheric Chemistry and Physics, 15, 2723–2747, doi:10.5194/acp-15-2723-2015, http://www.atmos-chem-phys.net/15/2723/2015/, 2015.